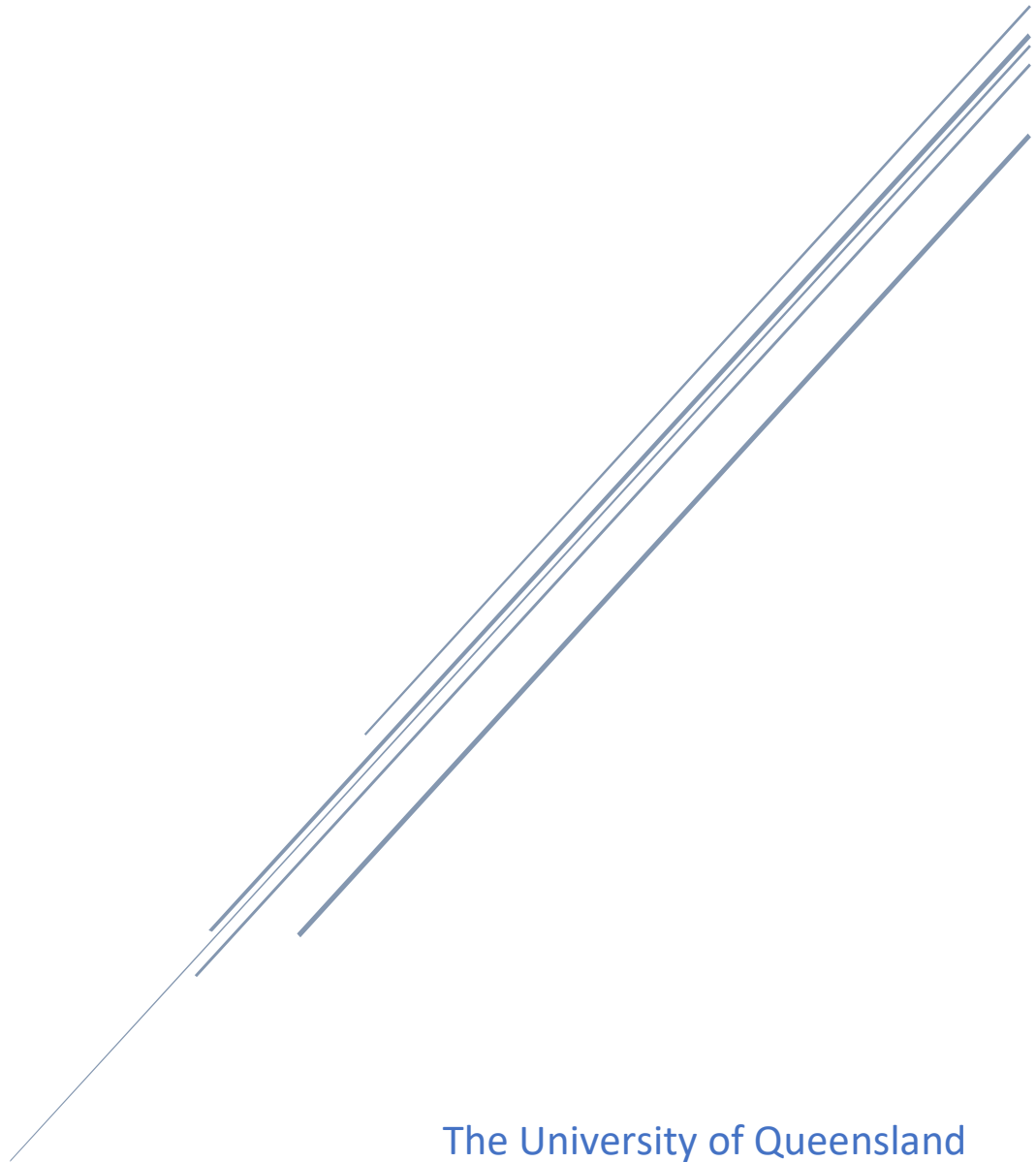# PROJECT REPORT

Utilising Google Earth Engine and Sentinel-2 Data for Snow cover mapping in the French Alps

The University of Queensland
School of Earth and Environmental Sciences
Rhys Persoon - 43533710

Contents

Research Report   43533710   Rhys Persoon

1.0 Abstract

Snow cover, in regions across the globe, plays an integral role in people's livelihoods, the economy, natural ecosystems and environments. As such the accelerating pace of climate change and associated loss of snow cover across the globe is becoming of increasing concern. In some parts of the world such as the European alps changes in snow cover levels and extent have been measured for hundreds of years utilising weather monitoring and other observational methods. In more recent times this has been undertaken utilising remote sensing practices to get a better picture of how snow cover behaves not only on a year-by-year basis but also over longer periods. It has been identified that snow cover levels and extent in the European alps are of concern and that studies into this area are essential. With the continuation of development of more advanced image processing techniques and improved capacity for data analysis more data can be analysed in a more timely, user friendly and accurate manner. This is enabled by improvements in software with one such example being the Google Earth Engine (GEE) platform which provides planetary scale analysis with a wide variety of datasets. This allows for more scalable and accessible solutions to not only global scientists but also decision makers and citizens.

This project has utilised the GEE platform to undertake an analysis of the extent of snow-covered area during the lifetime of the Sentinel-2A and 2B programs available on the GEE platform. This was done by utilising a classification method for snow cover extent with a strong theoretical background. This allowed for the classification of images over this five-year period by producing Normalised Difference Snow Indexes (NDSI) and classifying based on a cut-off value. In order to tackle many of the challenges to accurate snow mapping the classification methodology has taken into account factors such as cloud cover, water, vegetation and elevation. This has been carried out utilising representative images for each season of the year and has produced several mapping products as well as numerical outputs.

Assessments made of the accuracy of the methodology have shown that the classification was performed within acceptable levels of accuracy and is an effective method of performing snow cover mapping within the GEE environment which can be easily adapted for future use cases. While the study is unable to make any statements about long term trend, the overall trend through the study period was relatively stable, meaning no net increase or decrease in area and the spatial extent of snow cover was observed. The results of the study, have however, highlighted areas with the potential to provide reliable results for future longitudinal studies and provided an insight into the behaviour of snow cover over the study period in the study area. Finally, the study has also highlighted successes of the methodology utilised, as well as potential areas for improvement in the future.

Research Report   43533710   Rhys Persoon

2.0 Introduction

Over forty percent of the northern hemisphere during the winter season is covered by snow, making it the dominant land cover type during the season (Dietz, Kuenzer, Gessner and Dech, 2011). An essential component of the earths cryosphere, snow plays an important role in supporting and maintaining many natural global systems including protection of habitats, thermal regulation, maintenance of global albedo, and the global carbon cycle (Callaghan et al., 2011). Snow cover can be either permanent or seasonal, with many of the essential functions in the global system carried out by seasonal snowpacks. These snowpacks are not only vital to our natural environment, but also integral to sustaining life on the planet and have a considerable impact on a variety of human activities. It is estimated that one sixth of the global population relies on seasonal snowpacks and glacial melt as a source of fresh drinking water (Snapir et al., 2019) and in mountainous countries or regions such as Switzerland they can provide electricity through hydroelectric generation methods (Salzano et al., 2019).

Although snow cover plays an essential role in a variety of natural phenomena, and is essential to human activity, the effects of climate change have been impacting global snowpack levels. Studies have observed global decreases in snow cover since the 1960's, a trend forecast to continue (Dietz, Kuenzer, Gessner and Dech, 2011). While some areas are expected to be impacted more significantly than others, one key area of concern is the European Alps with some forecasts suggesting that Switzerland could see a decline between 7 and 25 percent by the end of the century (Klein et al., 2016). Not only is snowpack extent of serious concern, but also duration, with observed shorter snow seasons resulting from later first snow falls and earlier last snow days (Tsai, Dietz, Oppelt and Kuenzer, 2019).

Understanding the physical properties of snow including surface area, albedo, density, water content, crystal size and shape, permeability, thermal conductivity, and diffusivity is essential in determining how a snowpack interacts with its natural environment (Dong, 2018). By measuring and quantifying these parameters it is possible to determine how the snowpack effects the local and global environments and are often used as a basis for further modelling. Such modelling can help predict events including floods, drought, and famine (Jain, Goswami and Saraf, 2010), as well as factor into models effecting climate change and global radiation levels (Pulliainen et al., 2020). Historically the need for accurate and effective snow cover analysis has been identified, resulting in in-situ measurements at weather stations being conducted, with some records going back hundreds of years (Dong, 2018). In-situ measurement presents several challenges including maintaining uniformity in both location and method, spatially sparce data collection (Dong, 2018), and accessibility due to challenging or rough topography (Gaur et al., 2021). This has increasingly led to a

variety of remote sensing methods being used for many years with increasing accuracy and reliability as existing methods are built upon and refined (Gascoin et al., 2019).

3.0 Background & Literature

3.1 Statement of Problem

In general, the biophysical properties of snow cannot be quantified by a single variable. They are instead made up of a variety of smaller variables that are linked to the individual physical properties of snow cover. The quantifiable variables of these include snow covered area (SCA), fractional snow-covered area (fSCA), Snow Depth, Snow Water Equivalent (SWE), Liquid water content and Albedo (Gascoin et al., 2019). These variables provide a large quantity of useful information not only on our changing climate but also directly to companies, governments, and local service providers (Salzano et al., 2019). In general, each of the above-mentioned variables result in their own remote sensing product or graphical output and are generated using a variety of techniques. Of these variables it has been identified that the most important and the most widely studied are those of SCA and fSCA, primarily due to their wide variety of applications along with their use as inputs for a range of other modelling applications (Gascoin et al., 2019).

While it has been identified that there is substantial need to provide global products, similarly many of the above-mentioned use cases rely on frequent, high spatial resolution and accurate snow cover mapping which is able to be scaled and adapted in its context (Gascoin et al., 2019). Such mapping not only provides essential information to localised governments, organisations and consumers but also helps to increase the overall accuracy of SCA data by decreasing the chance of overestimation when compared with low spatial resolution techniques (Dietz, Kuenzer, Gessner and Dech, 2011). These products are also essential, when conducting analysis of seasonal snowpack change, to assess the impacts of broader trends such as climate change, with a specific need identified for further high-resolution mapping from the mid-2010s onwards over the European alps.

While many SCA methods and corresponding change analysis have been conducted at a relatively high resolution, it has been identified there is a need for further implementation and refinement of these methods. This is due to the challenging nature of the physical properties of snow oftenleading to a focus on a specific challenge including canopy cover (Rittger et al., 2020), cloud cover (Dozier, 1989) or the effects of water bodies (Gascoin et al., 2019) where each factor either masks or interferes with accurate classification (Gascoin et al., 2019). It is possible that with continued research in this area accuracy can be improved through the combination and refinement of methods.

3.2 Current Knowledge and Applications

Given the variety of challenges that are posed by the accurate remote sensing of snow cover it follows that there are a large variety of implemented methods that are carried out at both a global and localised scale (Dietz, Kuenzer, Gessner and Dech, 2011). Current knowledge and application on the remote sensing of snow cover usually fits into one of three main areas categorised by the sensor type used, these include Optical Imaging, Passive Microwave and Active imaging such as LiDAR and SAR (Dietz, Kuenzer, Gessner and Dech, 2011). These varied approaches are often due to the numerous physical properties of snow cover to which each different sensor is better suited. Optical methods are used to measure SCA, fSCA, and other factors, including impurity and grain size (Dietz, Kuenzer, Gessner and Dech, 2011). Passive methods often measure depth, density, and SWE by measuring microwave radiation attenuation due to the snowpack (Savoie, Armstrong, Brodzik and Wang, 2009), and active methods are used to measure a combination of variables or are combined with optical to improve accuracy and can be delivered using either airborne (Sokol, Pultz and Walker, 2003) or spaceborne platforms (Tsai, Dietz, Oppelt and Kuenzer, 2019). Each of these methods provide a variety of advantages and drawbacks due to the nature of the senser, with clouding in mountainous regions being a challenge for optical sensors, appropriate spatial resolution being a challenge for passive microwave and a combination of cost, resolution and availability often making active sensors difficult to implement (Dietz, Kuenzer, Gessner and Dech, 2011).

The project will be looking at SCA and therefore a focus will be placed on optical methods as they are often the most common and appropriate for measurement of this variable type (Dietz, Kuenzer, Gessner and Dech, 2011). Optical, being the most prevalent method of snow cover mapping has resulted in many global agencies producing products themselves which are published on their own hubs. These include NASA's Worldview Platform using MODIS data (Hall and G. A, 2021) and the European Space Agency's (ESA) Sentinel Hub using Sentinel-2 data (European Space Agency, 2015). In some cases, image providers also include a band within their imagery products such as the snow probability band provided with Sentinel-2 data generated by the Sen2Cor processor (Louis, Devignot and Pessiot, 2021). In addition to this several smaller research groups undertake classification using a variety of optical sensors, however at higher resolutions the two most common are the Landsat and Sentinel Programs (Gascoin et al., 2019).

While a variety of classification methods have been utilised including supervised, unsupervised, and spectral similarity (Salzano et al., 2019) the most widely used and most reliable is the Normalised Difference Snow Index (NDSI) method. This is often combined with a wide variety of other parameters and methods to increase accuracy (Dietz, Kuenzer, Gessner and Dech, 2011). Many of the current methods build upon the work of Dozier (1989) where such methods were used to

identify and classify snow cover. Additional parameters and methods are often aimed to address key issues relating to the physical or spectral properties of snow cover including the masking of cloud and canopy cover (Rittger et al., 2020), spectral similarities to certain cloud types most notably upper tropospheric cirrus clouds (Dong, 2018), and the prevalence when utilising NDSI of erroneously classifying turbid water bodies, commonly including rivers and lakes (Gascoin et al., 2019). Methods to deal with these issues are often widely varied including the use of masking for a variety of landcover types (Rittger et al., 2020), inclusion of Digital Elevation Models (DEM) (Baral and Gupta, 1997) and classification methods to estimate snow cover beneath clouds (Dietz, Kuenzer, Gessner and Dech, 2011).

It is also important to consider the implementation method used. In many cases classification has occurred either using individual software-based approaches such as ENVI or the Sentinel Application Platform (SNAP) (Kokhanovsky et al., 2019), Open-Source methods utilising Python as a coding basis and various toolboxes and libraries including GDAL (Gascoin et al., 2019) and the use of online platforms such as Google Earth Engine (GEE) (Irshad, Malik and Khalil, 2019). Despite the relative accessibility of GEE and ease of use with the provision of analysis ready data and planetary scale analysis delivered by access to cloud base computing, GEE is one of the least common methods with relatively few studies and processes developed utilising the platform (Zhang et al., 2020).

3.3 Aims and Objectives

This project aims to implement a classification algorithm to map snow extent at a relatively high spatial resolution of 20m and assess total seasonal SCA in the European alps from the mid-2010s onwards. To do this the French alpine region to the south of Genève and east of Lyon has been chosen, and the GEE platform selected for analysis. To meet this aim three main objectives have been set out. First is to implement an effective and accurate classification method to classify snow within the GEE Environment. Second is to select and accurately classify appropriate imagery from the sentinel-2 archive over the lifetime of the mission to allow for change analysis. Finally, to produce useful products and outputs for further analysis including change analysis and mapping outputs.

The decision to select GEE was based on the many merits of the package including scalability, accessibility, variety of data sources, computing power and potential for future work (Zhang et al., 2020). In addition to this GEE has been identified as having low levels of use for the purposes of snow cover mapping and as such requires further development and research in this specific area.

4.0 Data and Methodology

4.1 Data

4.1.1 Study Area

The study area selected is located in the southeast of France in the French alpine region. The site is situated south of Genève and east of Lyon and encompasses the city of Grenoble and major town of Chambéry. The site was selected based on its topographic features and variety of terrain types. The study areas include highly mountainous regions at high elevation which maintain snow cover for an extended period of time, moderate elevation locations with variable snow conditions (Olefs, Fischer and Lang, 2010), as well as lower elevation, relatively flat areas, in which towns and cities are constructed as well as farmland. The region also includes multiple lakes and ski resorts, each of which create unique surfaces with regard to the remote sensing of snow cover (Gascoin et al., 2019).

In addition to the unique topographical features of the landscape, the region was selected as it has been identified, as with other large parts of the European alpine region, as suffering from reduced snow cover and snow extent loss due to the effects of climate change (Klein et al., 2016). As such research and accurate snow cover mapping in this geographic region are essential to understanding these processes (Dong, 2018). Snow cover mapping in this region is also essential for a variety of other purposes including both commercial and for use by the general population. In line with this need, the region provides in situ snow monitoring utilising weather monitoring ground stations. As a result, selection of this site was made based on a combination of all factors including commercial, research, geographical features and availability of reference data. The specific study area which has been selected has been outlined in figure 4.1.
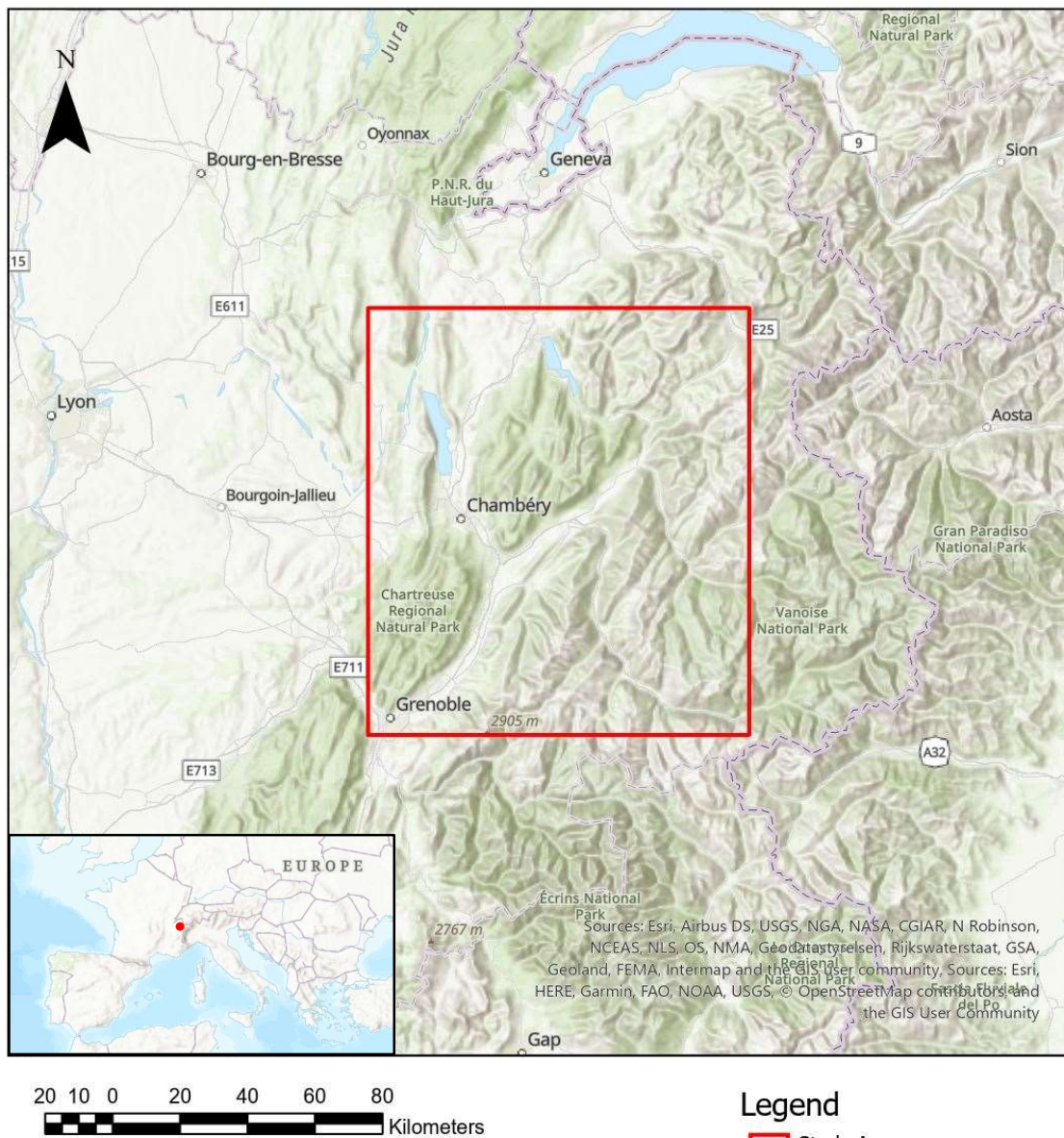
FIGURE 4.1 – STUDY AREA OUTLINED IN RED SHOWING RELATION TO MAJOR POPULATION CENTRES GENÈVE AND LYON

4.1.2 Selected Imagery Data Set

To meet the project objectives the properties of snow cover have been assessed and a sensor suite with appropriate Spectral, Radiometric, Spatial and Temporal dimensions has been selected to undertake the classification. The sensor selected to complete the project is that of the MSI onboard Sentinel-2 operated by ESA, the specific product selected is the Level 2A output. This data has been fully radiometrically and geometrically corrected using ESA's Sen2Cor processer and has therefore been selected as it is analysis ready (Louis, Devignot and Pessiot, 2021). Below in tables 4.1, 4.2 and 4.3 a theoretically ideal sensor has been presented for the project alongside the properties of the

Research Report   43533710   Rhys Persoon

MSI as well as an overview of each of the MSI's bands and additional bands provided. It is also important to note that the Sentinel-2 Level 2A product includes a wide variety of usual image properties and metadata which can be utilised for image selection and analysis purposes (European Space Agency, 2015).

REQUIREMENT	IDEAL DATASET	SENTINEL-2A AND 2B (MSI)
SPECTRAL	Visible, Near-Infrared (NIR) and Short Wave Infrared (SWIR)	Visible, NIR, SWIR
RADIOMETRIC	12 - Bit	12 - Bit
SPATIAL	10-20m	10m – Visible, NIR 20m – SWIR
TEMPORAL	Revisit Time of 5-10 days Operation 2010's onwards	5 days Operation 2015 onwards

TABLE 4.1 – THEORETICALLY IDEAL DATASET ALONGSIDE SENTINEL-2 DATASET (EUROPEAN SPACE AGENCY, 2015)

BAND NUMBER	DESCRIPTION	WAVELENGTH (MICROMETERS)	SPATIAL RESOLUTION
BAND 1	Aerosols	S2A – 443.9nm S2B – 442.3nm	60m
BAND 2	Blue	S2A – 496.6nm S2B – 492.1nm	10m
BAND 3	Green	S2A – 560nm S2B – 559nm	10m
BAND 4	Red	S2A – 664.5nm S2B – 665nm	10m
BAND 5	Red Edge 1	S2A – 703.9nm S2B – 703.8nm	20m
BAND 6	Red Edge 2	S2A – 740.2nm S2B – 739.1nm	20m
BAND 7	Red Edge 3	S2A – 782.5nm S2B – 779.7nm	20m
BAND 8	NIR	S2A – 835.1nm S2B – 833nm	10m
BAND 8A	Red Edge 4	S2A – 864.8nm S2B – 864nm	20m
BAND 9	Water Vapor	S2A – 945nm S2B – 943.2nm	60m
BAND 11	SWIR 1	S2A – 1613.7nm S2B – 1610.4nm	20m
BAND 12	SWIR 2	S2A – 2202.4nm S2B – 2185.7nm	20m

TABLE 4.2 – DESCRIPTION, WAVELENGTH AND PIXEL SIZE OF SENTINEL-2 DATA PRODUCTS (LOUIS, DEVIGNOT AND PESSIOT, 2021)

BAND NAME	DESCRIPTION	SPATIAL RESOLTUION
AOT	Aerosol Optical Thickness	10 meters
WVP	Water Vapor Pressure	10 meters
SCL	Scene Classification Map	20 meters
TCI_R	True Colour Image, Red channel	10 meters
TCI_G	True Colour Image, Green channel	10 meters
TCI_B	True Colour Image, Blue channel	10 meters
MSK_CLDPRB	Cloud Probability Map	20 meters
MSK_SNWPRB	Snow Probability Map	10 meters
QA60	Cloud Mask	60 meters

TABLE 4.3 – ADDITIONAL BANDS PROVIDED IN THE SENTINEL-2 DATASET (LOUIS, DEVIGNOT AND PESSIOT, 2021)

4.1.3 Additional Datasets Utilised

In addition to the image dataset utilised, a Digital Elevation Model (DEM) Dataset has been used in the classification process. The dataset selected for this purpose was the NASA SRTM Digital Elevation 30m. This dataset is available for utilisation with the same method as the Sentinel-2 data and can be imported through GEE. This dataset was selected due to its relatively high spatial resolution compared with other DEM datasets available through GEE, its global coverage, and reliability (Farr et al., 2007). The dataset consists of a single elevation band as outlined in table 4.4.

BAND NUMBER	DESCRIPTION	MINIMUM VALUE	MAXIMUM VALUE	SPATIAL RESOLUTION
BAND 1	Elevation	-10m	6500m	30

TABLE 4.4 – BAND PROVIDED BY THE NASA SRTM DIGITAL ELEVATION 30M DATASET (NASA, 2015)

4.2 Methodology

4.2.1 Overview of Processing Sequence

All steps with the exception of partial accuracy assessment were undertaken in the GEE environment, this included importation, filtering, selection, masking, generation of indices, classification, accuracy assessment, generation of relevant statistics and generation of output maps. The flowchart below in figure 4.2 provides a high-level overview of each of the steps taken in the processing sequence.
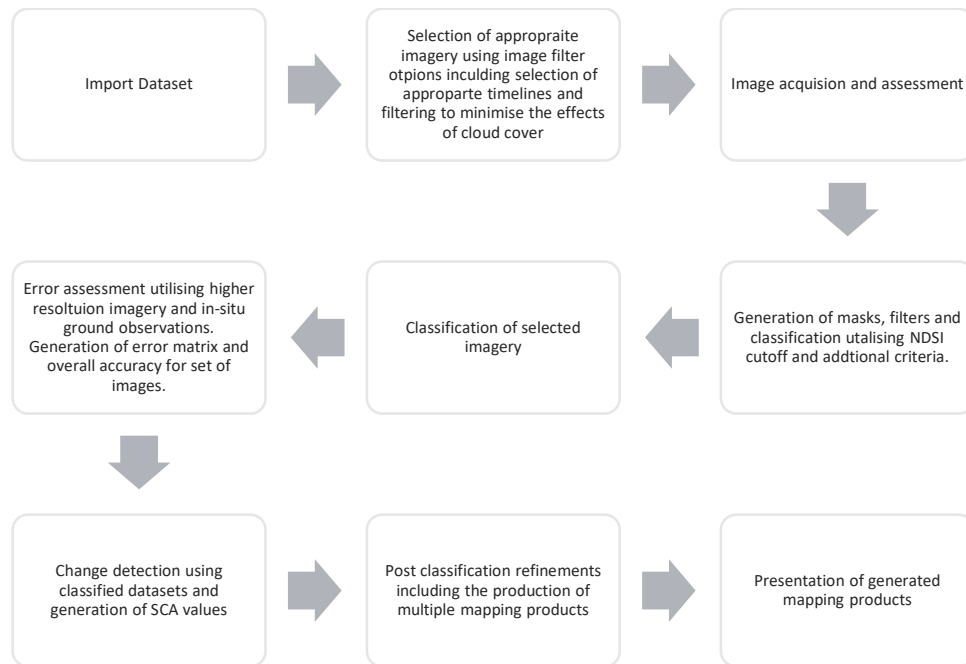
Research Report   43533710   Rhys Persoon

4.2.2 Image Selection, Acquisition and Filtering

The first step undertaken was to select, import, and filter the selected dataset into an image collection within the GEE environment to allow for processing to take place. As previously discussed the Sentinel-2 Level 2A dataset had been selected, this dataset was imported from the GEE data catalogue. Upon importation into the GEE environment the entire dataset is loaded with all images, as a result the next step completed was that of filtering the dataset to generate images for classification.

In order to meet the objectives of the project an image was used to represent each calendar season of the year from the beginning of the sentinel program until the most recent fully completed season. In addition to this a key challenge to snow cover mapping is dealing with cloud cover in an appropriate manner (Dozier, 1989). The process of filtering and generating images to represent each of the seasons, as well as the process of removing potential classification issues due to cloud cover, were dealt with in this initial stage.

In order to effectively do this the dataset was first filtered into three monthly segments, this provides all images from the sentinel-2 dataset within the set time period generating an image collection that represents a set calendar season. This image collection was then filtered by cloud cover percentage so that only images below 30% cloud cover were included (Li et al., 2021). All images in the dataset were then cloud masked utilising the cloud mask band and a single composite image was generated based on a per pixel based median operation (Li et al., 2021). This was selected

due to the likelihood of a high impact of outlier events, for example a single snow day which melts within hours or days (Li et al., 2008). As a result the most relevant cloud free imagery of the study area for that time period can be generated.

The final result has been clipped to the study area and the cloud mask carried over to the final image, this represents areas which were covered by cloud in all images over the entire three month period.

FIGURE 4.3 – EXAMPLE OF A COMPOSITE IMAGE REPRESENTING A CALENDAR SEASON UTILISED FOR CLASSIFICATION, IMAGE DISPLAYED FROM WINTER 2022

Research Report   43533710   Rhys Persoon

4.2.3 Calculation of Relevant Indices

The snow cover classification method chosen relies on the generation of an NDSI for each image. This band will be the primary band that classification will be based on (Gascoin et al., 2019). An NDSI for the MSI sensor can be defined as:

$$NDSI = \frac{B3 - B11}{B3 + B11}$$

Where B3 refers to band 3 (green) and B11 refers to band 11 (SWIR) (Salzano et al., 2019).

In addition to this for the assessment of vegetation cover in the area, a factor which will affect the accurate assessment of snow cover, a Normalized difference vegetation index (NDVI) was used (Vizzari, Santaga and Benincasa, 2019). This band when added to the image is designed to give an indication of the degree of vegetation which could be obscuring or effecting the accurate classification of snow cover (Rittger et al., 2020). This is due to vegetation factors which reduce the effectiveness of the NDSI methodology when mixed with higher quantities of vegetation (Dietz, Kuenzer, Gessner and Dech, 2011). An NDVI for the MSI sensor can be defined as:

$$NDVI = \frac{B8 - B4}{B8 + B4}$$

Where B8 refers to band 8 (Near Infra Red) and B4 refers to Band 4 (Red) (Vizzari, Santaga and Benincasa, 2019).
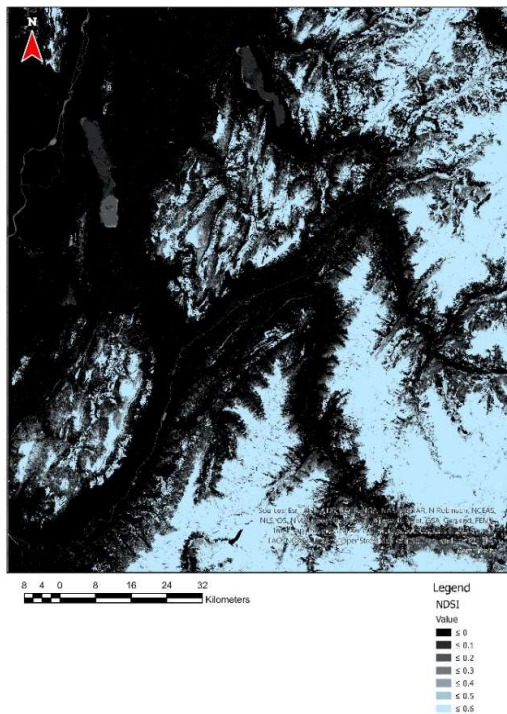

FIGURE 4.4 – EXAMPLE OF NDSI IMAGE UTILISED IN CLASSIFICATION, EXAMPLE FROM WINTER 2022
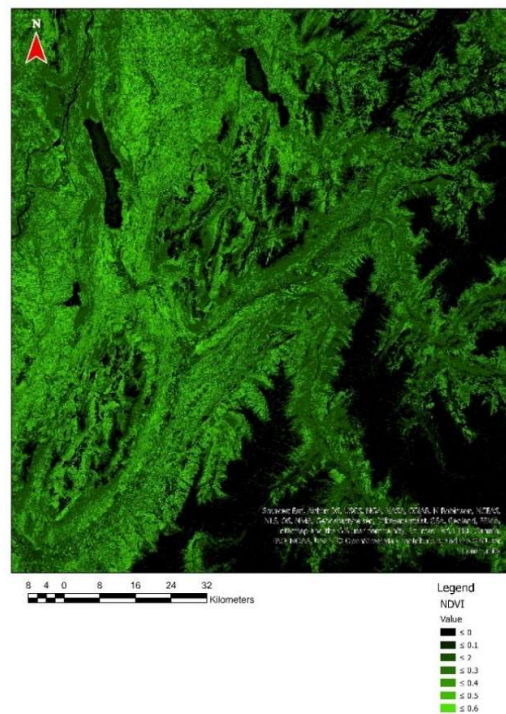
FIGURE 4.5 – EXAMPLE OF NDVI IMAGE UTILISED IN CLASSIFICATION, EXAMPLE FROM WINTER 2022

4.2.4 Classification Methodology

The classification methodology used utilises and builds upon the most widely employed method to determine SCA, this method also has the strongest theoretical background (Dietz, Kuenzer, Gessner and Dech, 2011). Therefore, an algorithm which primarily utilises NDSI to perform classification was used to complete the project. This was done by selecting a value above which a pixel will be classified as snow, the base NDSI value for this project was selected as 0.6 (Gascoin et al., 2019). The base cut off value adjusted was dependent on other variables which consider attributes effecting the ability to complete an effective SCA classification (Gascoin et al., 2019).

The other variables selected to be taken into account when selecting an appropriate cut off were those of presence and absence of vegetation, water bodies and elevation in the form of a calculated snowline. Vegetation quantity was assessed on a sliding scale with a reduction in required NDSI where NDVI values indicated high levels of vegetation (Rittger et al., 2020). The tendency of NDSI to misclassify water was reduced by the additional requirement to return a certain reflectance in the red band. This was selected due to the differing spectral properties of water and snow in the red band (Gascoin et al., 2019) this can be seen in the figure 4.6 below showing actual snow and water samples from the study area.
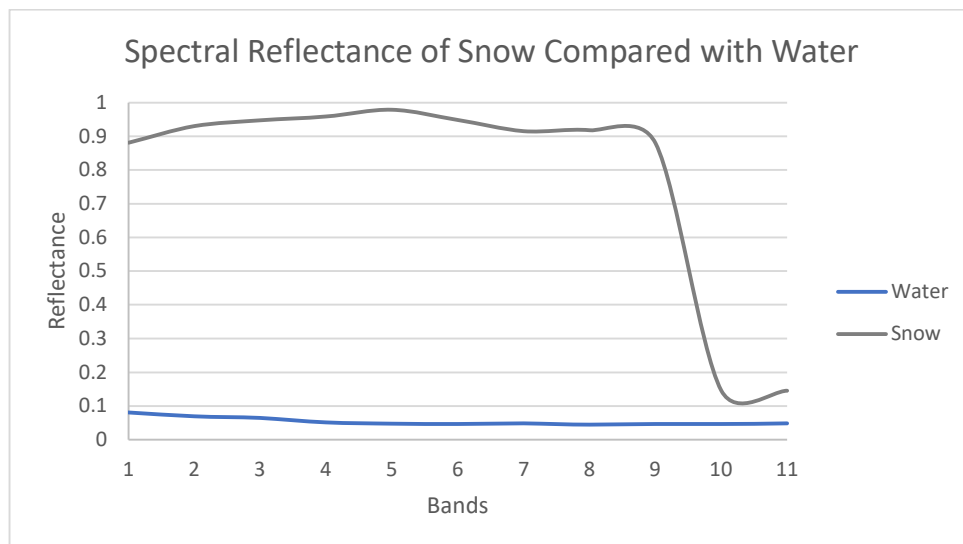

FIGURE 4.6 – SPECTRAL REFLECTANCE OF SAMPLE SITE OF SNOW VS SAMPLE SITE OF WATER FROM STUDY AREA FROM SENTINEL 2 MSI

The final criteria for classification was the inclusion of the assessment of elevation. This was utilised as snow is more likely to occur and therefore the threshold for classification can be lowered when above a certain altitude (Gascoin et al., 2019). Past studies have utilised this method and selected thresholds utilising the Snowline (Gascoin et al., 2019). The project utilised this established method

of assessment and due to the seasonal nature of each image it was identified that the snowline would need to be calculated uniquely for each image. This was done similarly utilising an established process, to calculate snowline the number of pixels classified as snow using the most conservative cut-off was grouped into 200m elevation groups and compared with other elevation groups. The point at which the SCA dropped below 50% was determined to be the snowline (Gascoin et al., 2019). This elevation was then used in the classification methodology with a less conservative NDSI threshold applied when classifying pixels above the snowline (Gascoin et al., 2019). Elevation groups for the study area have been shown in figure 4.7 below.
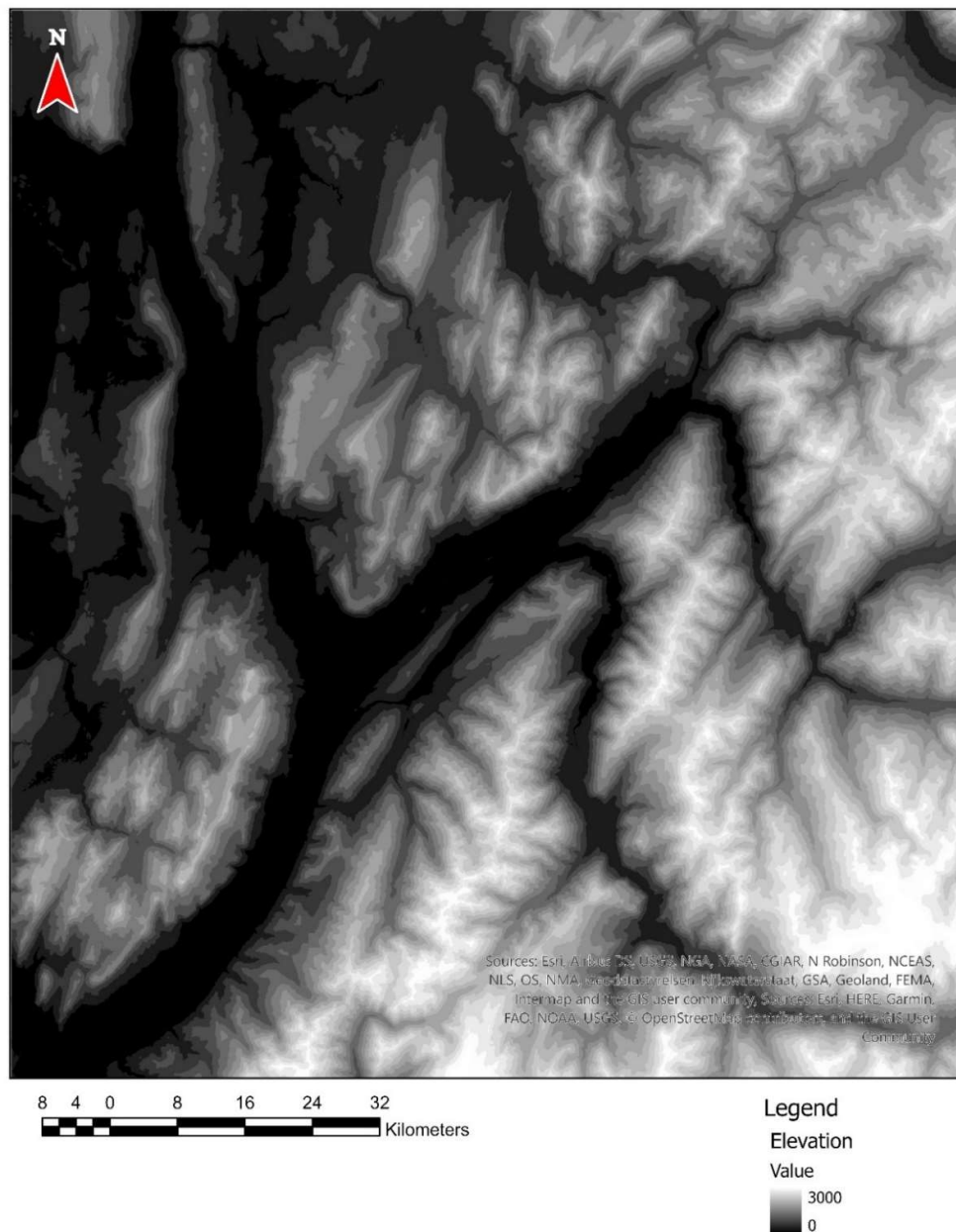

FIGURE 4.7 – IMAGE UTILISED FOR GROUPING OF ELEVATION VALUES IN 200M BANDS

The combination of the above requirements were implemented by generating a newly classified binary image with values representing no snow cover and snow cover. This process was then carried out across all images in the image collection allowing for snow cover mapping for each season across all years in the collection. An example of this final result can be seen in figure 4.8.
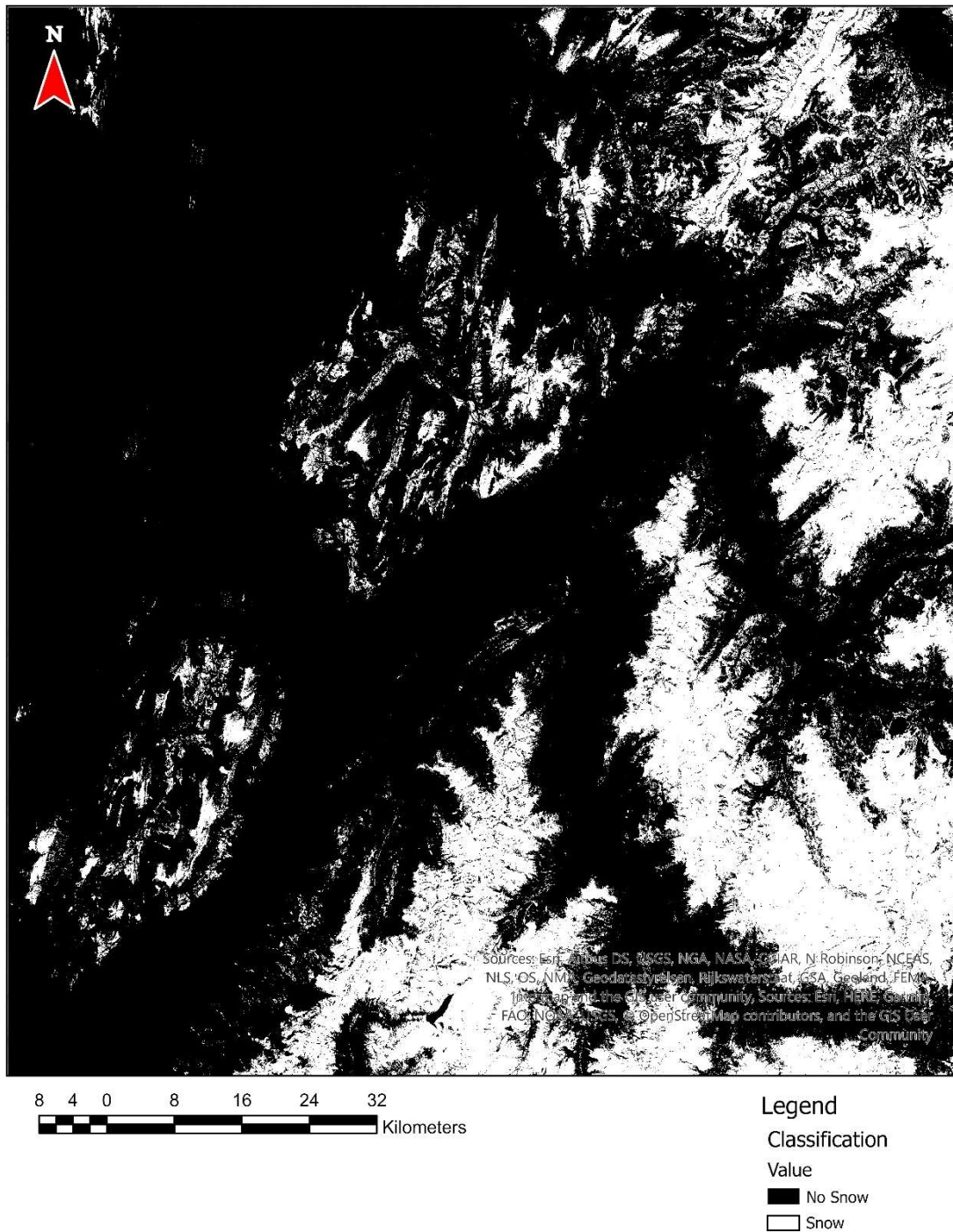

FIGURE 4.8 – EXAMPLE OF FINAL CLASSIFIED SNOW IMAGE, IMAGE SHOWS CLASSIFICATION FOR WINTER 2022

4.2.5 Accuracy Assessment

Following the classification, an accuracy assessment was undertaken using a combination of in-situ monitoring and higher resolution imagery (Gascoin et al., 2019). In-situ data was derived from snow measurements taken from weather monitoring stations across the chosen site and provided by Météo-France (Météo-France, 2017), higher resolution imagery is to be selectively sourced from Planet Labs data. Error assessment was carried out using a contingency error matrix method for both cases with appropriate error assessment metrics generated (Kumar, Husain, Singh and Kumar, 2018).

The Météo-France data was collected from the Météo-France website with data being downloaded to represent each season. This data was then averaged to determine if snow was measured as being present across this time period and then subsequently classified into a binary snow or non snow classification. This table was then loaded into Google Earth Engine in a CSV format and used to generate a contingency error matrix and overall accuracy statistic for all images in the series (Kumar, Husain, Singh and Kumar, 2018). As such the accuracy of all images have been assessed utilising this method. In addition to this it is important to note that the data collected by Météo-France is spot location data and as a result is collected at a specific location (Météo-France, 2017) and therefore will be located within each of the classified pixels, this can also potentially affect the outcome of the accuracy assessment (Gascoin et al., 2019).

For the second method utilising planet data, a segment of the image was selected for accuracy assessment as seen in figure 4.9 along with 4 output images, one representing each season. This is due to limitations to freely available Planet Labs data for research purposes.
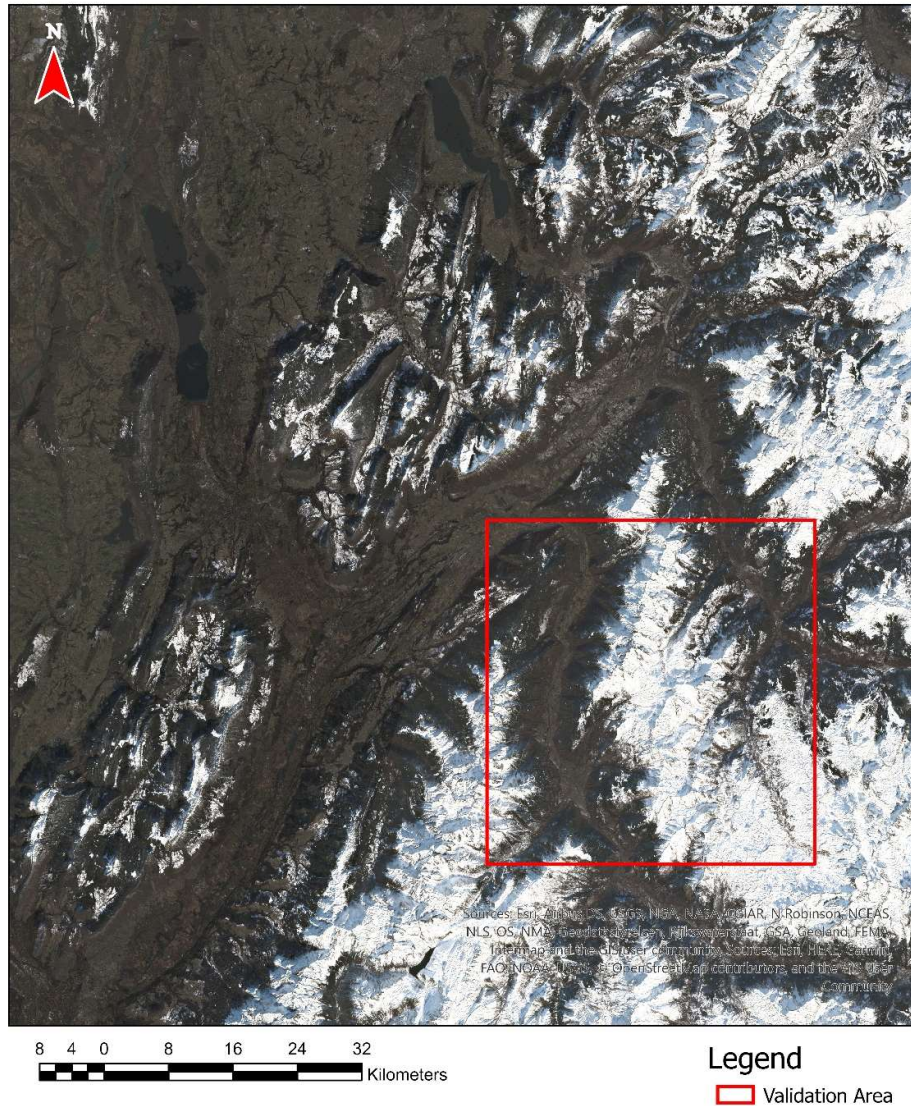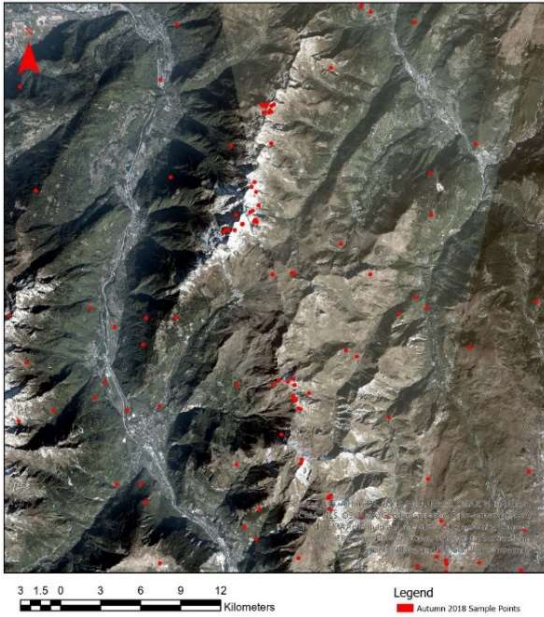
FIGURE 4.9 – SUB AREA USED FOR ACCURACY ASSESSMENT AND VALIDATION WITH PLANET DATA AND ENVI SOFTWARE

Both images were then imported into ENVI software where an error assessment was undertaken. This method also utilised a contingency error matrix with output statistics generated through ENVI (Kumar, Husain, Singh and Kumar, 2018) utilising a ground truth ROI methodology with at least 50 ground truth points per class with values for each point derived from the planet imagery (Congalton, 1991). For this method a stratified random sample was utilised as this will yield the most appropriate outcome and is considered to be one of the most statistically sound methods for such an assessment (Boschetti, Stehman and Roy, 2016). The points and Planet imagery utilised can be seen in figure 4.10 below.

Research Report   43533710   Rhys Persoon

Autumn 2018
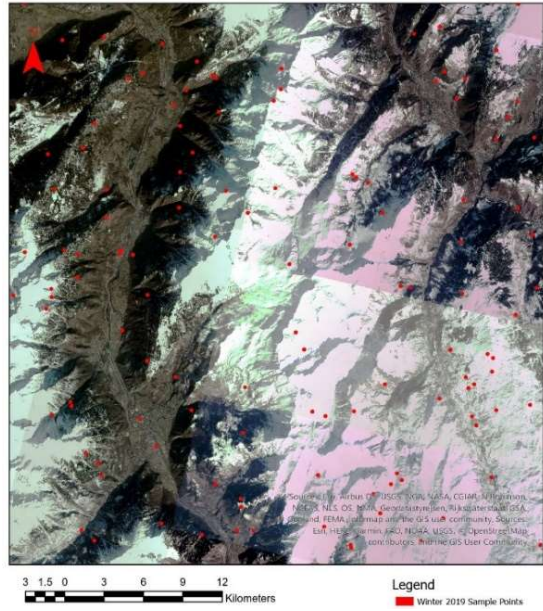
Winter 2019
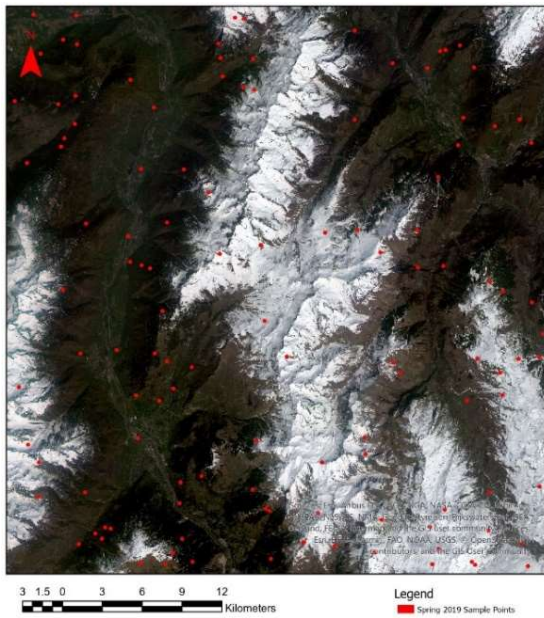
Spring 2019

Summer 2019

FIGURE 4.10 – SAMPLE POINTS UTILISED FOR ACCURACY ASSESSMENT WITH CORRESPONDING IMAGES FROM PLANET

Research Report   43533710   Rhys Persoon

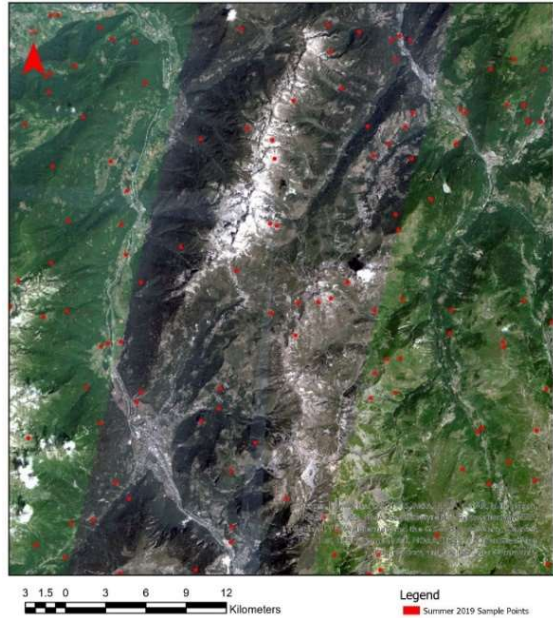It is important to undertake both methods of error assessment due to a combination of limitations with both methods. In the case of utilising the Météo-France data only data contained within the study area can be utilised amounting to a total of 20 points, the set location and reliability of the data for certain regions and time periods may lead to inaccurate accuracy reporting. For example, for some seasons, predominantly summer months, no data is collected by large numbers of the monitoring stations (Météo-France, 2017). While for the Planet imagery accuracy assessment can only be undertaken for a set number of images.

4.2.6 Generation of Outputs and Statistics

Once the accuracy of the classification had been generated, change detection was undertaken across all selected Images. This allowed for the generation of multiple mapping products as well as numerical and graphical representations of SCA. The statistic for SCA can be defined by the formula below:

$$SCA = \left(\frac{N_S}{N_T}\right) \times 100\%$$

Where N_S is the number of snow-covered pixels and N_T is the total number of pixels receiving a binary classification, meaning it was classified as snow or non-snow, excluding other cover types such as identified cloud cover or water mask (Dong, 2018). The SCA statistic will be the predominant output for each of the images along with individual image products, this is due to the variability in cloud cover between images. This is due to each image containing a variety of different quantities of cloud cover and therefore cloud cover masks. This means not all images will have the same total number of pixels classified. The SCA statistic helps adjust for this by calculating snow cover based only on the total number of pixels classified (Dong, 2018). It should also be noted that due to limitations on processing requirements within the GEE environment (Zhang and Zhang, 2020) SCA was required to be conducted at a reduced scale, for these purposes a scale of 100m was selected, these changes only effect SCA output percentages and not mapping product results.

4.2.6 Image Aggregation and Production of Final Mapping Products

In order to best assess the results of the classifications the final images were aggregated together. This resulted in two major outputs, the first being an aggregation of all output images showing the number of seasons an area has been covered by snow over the entire study period. The second being seasonal based aggregations, to better show variability within seasons over the study period. This was completed by selecting individual images for the relevant output and performing a band math sum operation.

5.0 Results

The project delivers several specific outcomes linked to the project aims and objectives. These include the delivery of an effective and accurate method for classifying snow cover within the GEE Environment. The generation and analysis of several SCA products including mapping, numerical quantification and graphical representations and analysis of these products. The outputs that have been delivered come in a variety of formats, while it is possible to generate individual classifications for each of the images this would only be useful for looking directly at the context of a year or season as the individual image outputs have been aggregated together into an individual image. This has been done for individual seasons and for the entire period. This can give a better idea of snowpack change over the study period. In addition to this Snow Covered Percentages have been provided for each individual image to allow for more in-depth comparison and these figures have been plotted for a visual representation on the seasonal cycle as well as changes between each of the seasons.

5.1 Aggregated Results

The below mapping products show aggregated outputs for each of the specified criteria.

Complete Timeframe

FIGURE 5.1 – AGGREGATION OF ALL IMAGES WITHIN THE OUTPUT DATASET TO DISPLAY THE NUMBER OF SEASONS THAT
A PIXEL WAS CLASSIFIED AS COVERED IN SNOW

The above map in figure 5.1 displays all of the classified images aggregated into a single image, this represents the number of seasons over the entire timeframe of the study including all four seasons and all years. The maximum total possible is 19 different seasons with the lowest being 0, each class represents the lower limit for the number of seasons. The image gives insight into which areas have

been permanently covered for the study period, which experience frequent snowfall or are frequently covered for the winter months, as well as the greatest possible extent of snow coverage over the study period, and in which areas it is unlikely to see snow coverage during a season.

Autumn

FIGURE 5.2 – AGGREGATION OF ALL CLASSIFIED IMAGES WITHIN THE DATASET FOR THE AUTUMN SEASON

The above map in figure 5.2 displays all the classified images from the autumn season to a single image. The image represents the number of Autumn seasons over the 5 year study period that were snow covered. This map is therefore useful to provide insight to the maximum and minimum extents of snow cover in Autumn over the study period. The maximum possible being 5 and minimum 0.
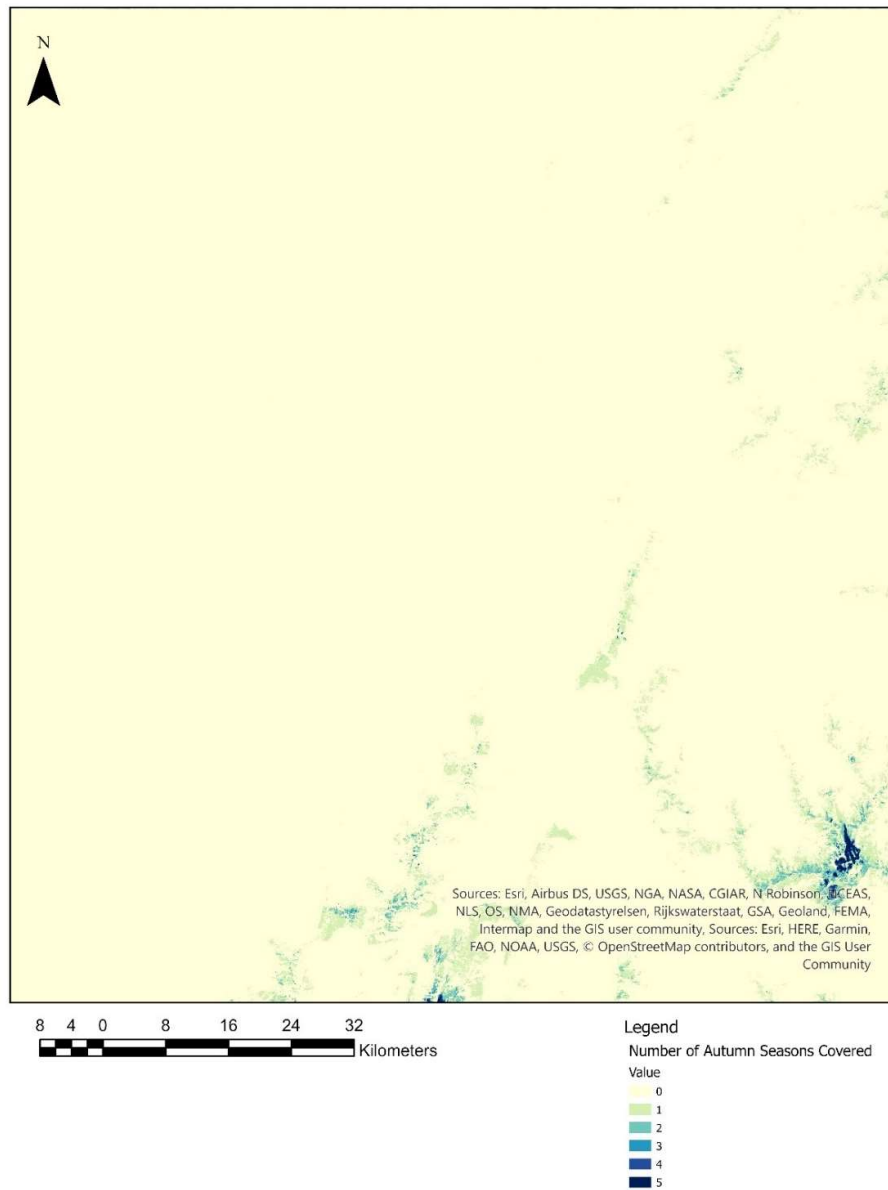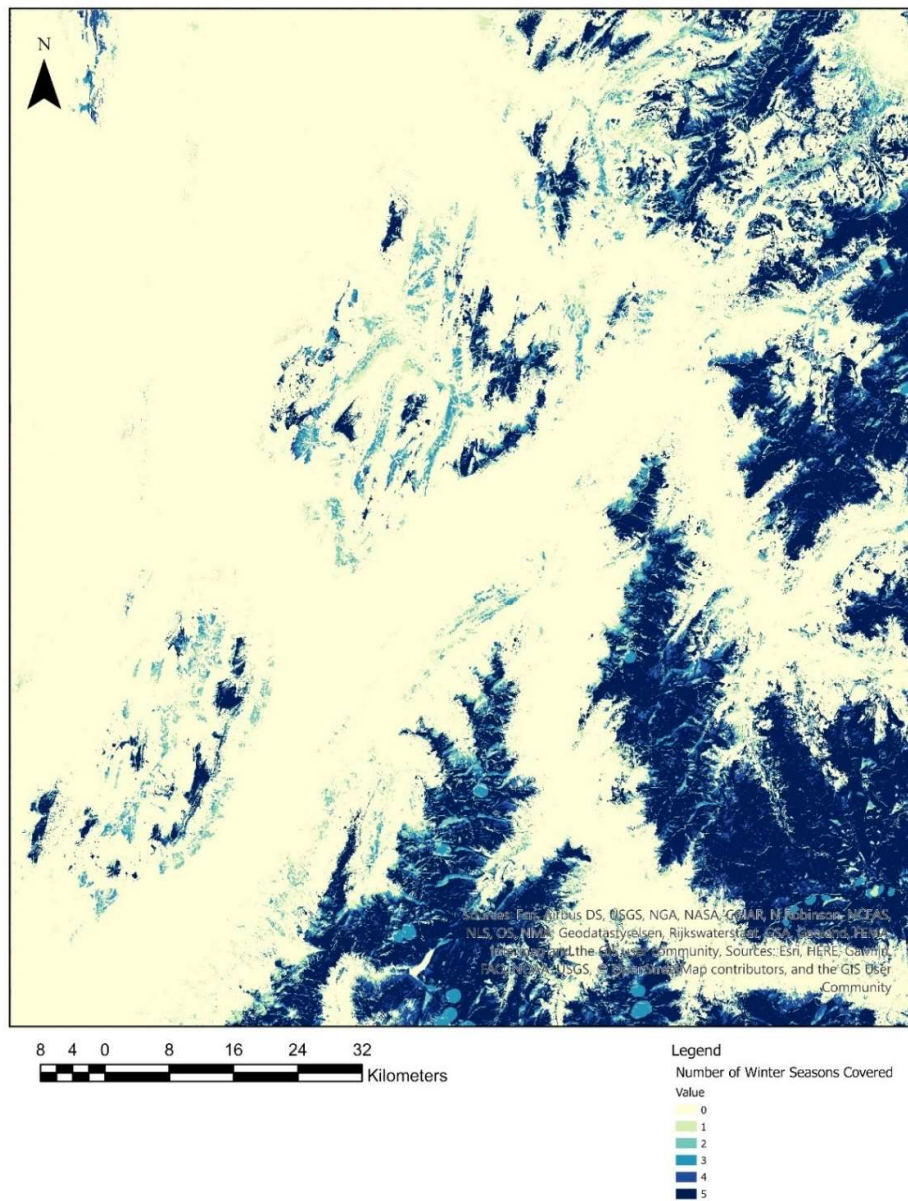
Winter

FIGURE 5.3 – AGGREGATION OF ALL CLASSIFIED IMAGES WITHIN THE DATASET FOR THE WINTER SEASON

The above map in figure 5.3 displays an aggregation of all output snow cover images for the winter season over the study period. The maximum possible number of seasons being 5 and the minimum being 0. The map provides insight into extent of regular snow cover during the season as well as areas which are covered in moderate and higher snowfall seasons over the study period. It should be noted that small areas of the image below show lower seasonal counts in distinct patches, these areas have been affected by the lack of data due to cloud masking. These areas were not masked out because in doing so the relevant data from all seasons would be affected therefore removing valid data.

Research Report   43533710   Rhys Persoon

FIGURE 5.4 – AGGREGATION OF ALL CLASSIFIED IMAGES WITHIN THE DATASET FOR THE SPRING SEASON

The above map in figure 5.4 shows the aggregation of all images within the dataset for the Spring Season with the minimum being 0 and maximum being 4. There is one less season in this dataset owing to the time of year at completion of the analysis and the earliest start date of data availability being a full summer season. This image provides insight into the number of seasons snow was present in spring as well as the reliability of snow cover in the area and snow cover characteristics during the study period. It would be also noted that small areas of this image also suffer from the effects of cloud masking.
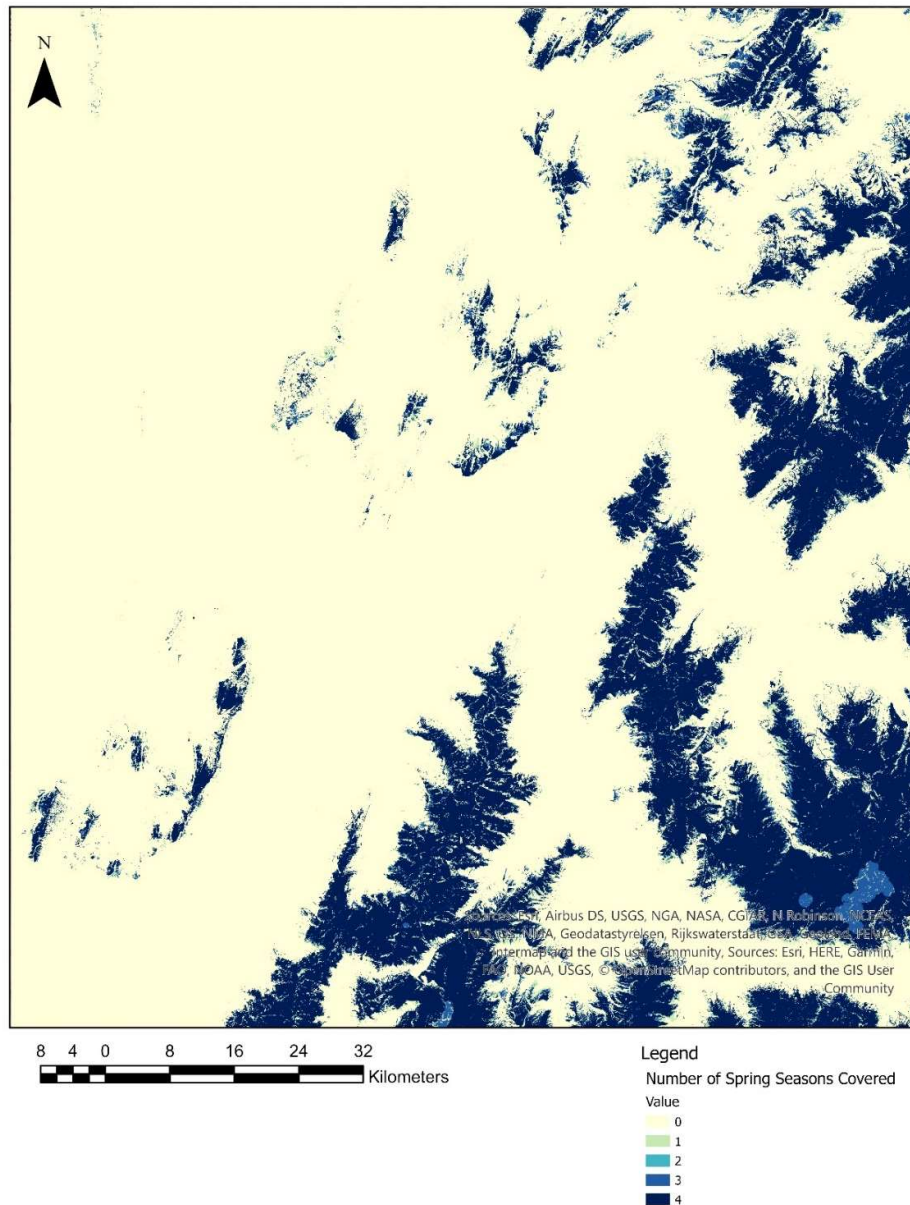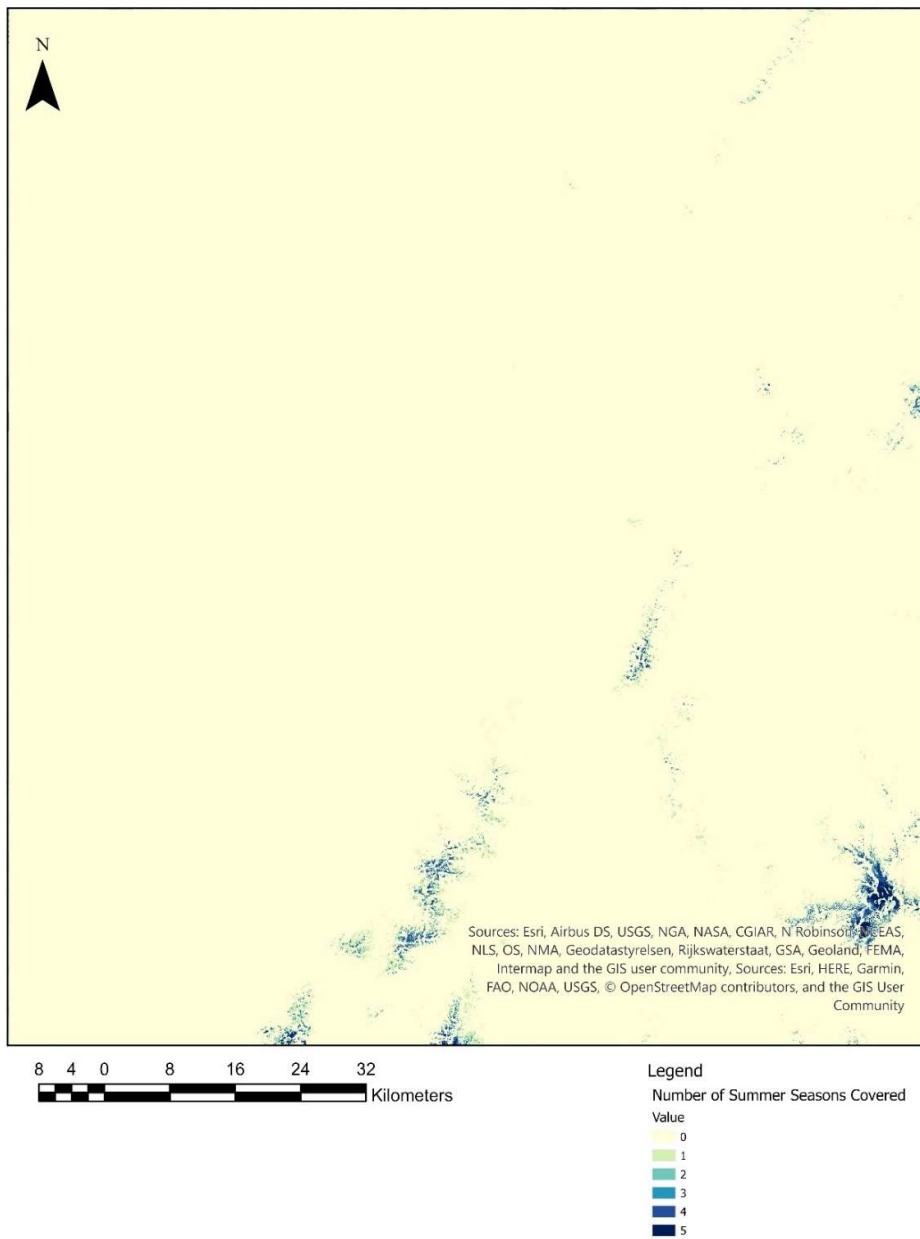
Summer

FIGURE 5.5 – AGGREGATION OF ALL CLASSIFIED IMAGES WITHIN THE DATASET FOR THE SUMMER SEASON

The above map in figure 5.5 shows the aggregation of all classified images for the summer seasons with the minimum possible being 0 and maximum being 5. This image similarly to the other provides an insight into the snow cover extent and permanence during the summer seasons.

5.2 Snow Covered Area (SCA)

Snow covered area has been calculated based on the methodology outlined in the above methods section. As discussed this methodology allows for better estimation of snow cover levels as a portion of the entire area. This also provides insight into good seasons, poor seasons and seasonal average and trends for the study period.

YEAR/SEASON	WINTER	SPRING	SUMMER	AUTUMN
2017			0.135	0.598
2018	20.959	19.285	0.423	0.196
2019	27.164	19.177	0.348	0.141
2020	21.954	15.742	0.334	1.552
2021	24.109	19.436	0.734	0.388
2022	24.493			

TABLE 5.1 – ALL CALCULATED SCA VALUES FOR EACH CLASSIFIED IMAGE OUTPUT.

The below chart (figure 5.6) has been generated based on the above snow cover values, each point has been plotted and a line fitted to indicate snow cover cycles over the period of study. This helps give an overall indication of snow cover trend over the study period as well as change.
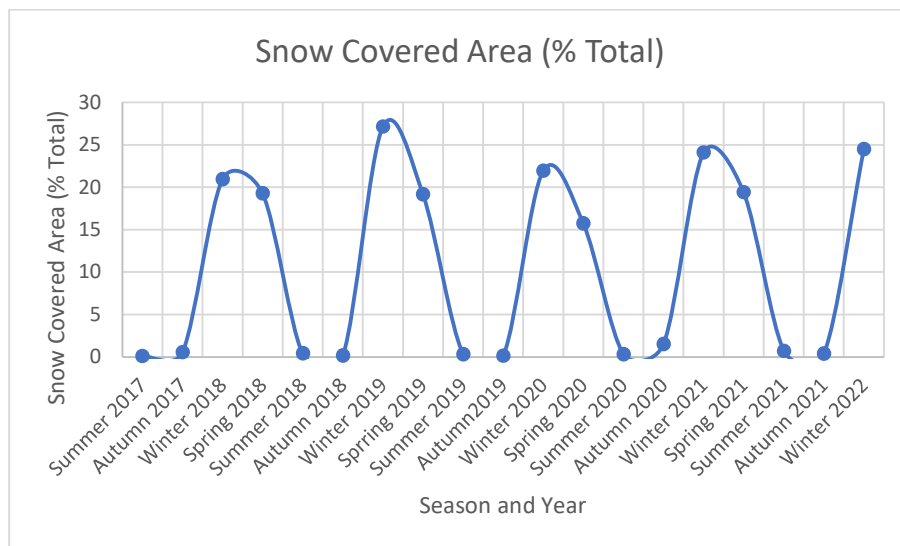
FIGURE 5.6 – SCA PERCENTAGES PLOTTED BY SEASON WITH LINE FITTED TO SHOW SCA SEASONAL CYCLES

The below graph (figure 5.7) also generated from the above table displays plotted snow cover levels for each season over an individual year and compares them with all other years during the study period. This allows for better comparisons of potential changes and highlights good and poor years. It also provides and indicative profile of a year's snow cover over the study area. In this case the year 2022 has been excluded as the only data recorded was for winter meaning there is no available profile segment.

FIGURE 5.7 – PROFILE OF SCA FOR EACH YEAR DURING THE STUDY PERIOD (EXCLUDING 2022) PLOTTED BY SEASON

5.3 Accuracy Assessment

The below tables show the outcomes of the error assessment for the four selected images, one representing each season. With all overall accuracies being above 90% all assessed images fall within an acceptable range for accuracy. Of these It can be seen that Summer provi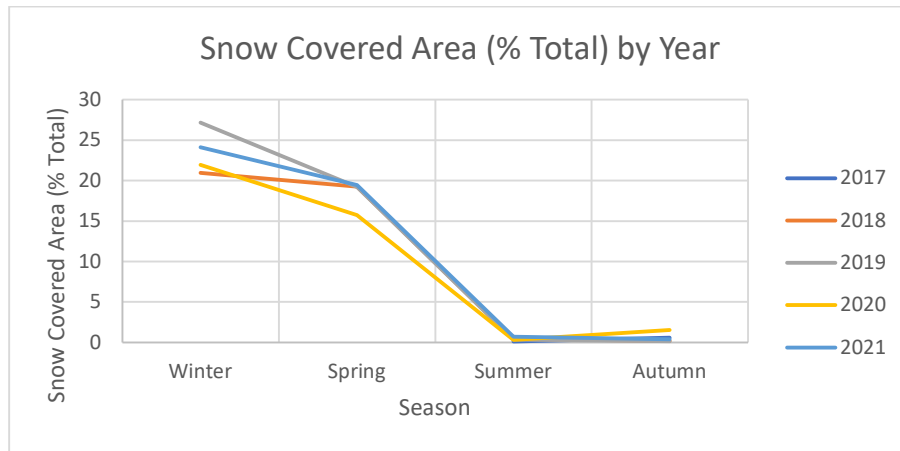ded the highest overall accuracy and Winter the lowest. In addition to this the overall Commission and Omission error as well as Producer and User accuracy has been displayed for each image along with the number of sample points all being 122 and the Kappa Coefficient.

AUTUMN 2018		
OVERALL ACCURACY	93.4426%	
KAPPA COEFFICIENT	0.8689	
SAMPLE POINTS	122	
COMMISSION & OMISSION ERROR		
	Commission(%)	Omission(%)
SNOW	8.20	5.08
NO SNOW	4.92	7.94
PRODUCER & USER ACCURACY		
	Producer Accuracy(%)	User Accuracy(%)
SNOW	94.92	91.80
NO SNOW	92.06	95.08

TABLE 5.2 – ACCURACY ASSESSMENT RESULTS FOR THE PORTION OF THE AUTUMN 2018 IMAGE ASSESSED

WINTER 2019		
OVERALL ACCURACY	90.1639%	
KAPPA COEFFICIENT	0.8028	
SAMPLE POINTS	122	
COMMISSION & OMISSION ERROR		
	Commission(%)	Omission(%)
SNOW	3.85	16.67
NO SNOW	14.29	3.23
PRODUCER & USER ACCURACY		
	Producer Accuracy	User Accuracy
SNOW	83.33	96.15
NO SNOW	96.77	85.71

TABLE 5.3 – ACCURACY ASSESSMENT RESULTS FOR THE PORTION OF THE WINTER 2019 IMAGE ASSESSED

SPRING 2019		
OVERALL ACCURACY	95.9016%	
KAPPA COEFFICIENT	0.9065	
SAMPLE POINTS	122	
COMMISSION & OMISSION ERROR		
	Commission(%)	Omission(%)
SNOW	2.63	9.76
NO SNOW	4.76	1.23
PRODUCER & USER ACCURACY		
	Producer Accuracy(%)	User Accuracy(%)
SNOW	90.24	97.37
NO SNOW	98.77	95.24

TABLE 5.4 – ACCURACY ASSESSMENT RESULTS FOR THE PORTION OF THE SPRING 2019 IMAGE ASSESSED

SUMMER 2019		
OVERALL ACCURACY	96.7213%	
KAPPA COEFFICIENT	0.9344	
SAMPLE POINTS	122	
COMMISSION & OMISSION ERROR		
	Commission(%)	Omission(%)
SNOW	1.64	4.76
NO SNOW	4.92	1.69
PRODUCER & USER ACCURACY		
	Producer Accuracy(%)	User Accuracy(%)
SNOW	95.24	98.36
NO SNOW	98.31	95.08

TABLE 5.5 – ACCURACY ASSESSMENT RESULTS FOR THE PORTION OF THE SUMMER 2019 IMAGE ASSESSED

Below the accuracy results from the confusion matrices for the ground monitoring stations have been presented. While it is not appropriate they be completely discarded it is likely that many of the results have been badly effected by outliers and missing, incomplete and unavailable data. The dataset used often had very few monitoring stations available during shoulder seasons with some as little as three stations out of the total twenty available in winter. This means that if as little as one datapoint is inaccurate or correctly identifies error, due to the very small sample size, this can affect the overall error levels by up to 33%. In addition to this there were often no monitoring stations available for summer seasons. While the data provides an insight to accuracy across the entire dataset it should not be relied upon to determine the accuracy of the classification. It should also be noted that due to the increased quantity of reliable observation points during the winter months these are often the most reliable and accurate measures of reliability, incidentally these are also the results that measure higher levels of accuracy.

SEASON	OVERALL ACCURACY (%)
SUMMER 2017	N/A
AUTUMN 2017	N/A
WINTER 2018	63.1579
SPRING 2018	46.6667
SUMMER 2018	N/A
AUTUMN 2018	N/A
WINTER 2019	78.9473
SPRRING 2019	57.1428
SUMMER 2019	100
AUTUMN2019	100
WINTER 2020	72.2221
SPRING 2020	N/A
SUMMER 2020	100
AUTUMN 2020	N/A
WINTER 2021	81.25
SPRING 2021	85.7143
SUMMER 2021	N/A
AUTUMN 2021	100
WINTER 2022	66.6667

TABLE 5.6 – OVERALL ACCURACY VALUES FROM CONFUSION MATRICES GENERATED FOR THE GROUND MONITORING STATIONS

6.0 Discussion

6.1 Analysis of snow cover change

Overall, the outputs from the project including the SCA percentages and the resulting aggregated snow cover maps can help give insight into the patterns of snow cover extent over the period studied. In general, by looking at the snow cover percentages in figure 5.6 the heavily cyclical nature of snow cover in this area is evident with snow cover dropping to almost 0% in the summer and autumn months and as high as 27% in Winter. While it is apparent that there can be large differences between snow cover extents in different seasons, representing poor and better seasons (Durand et al., 2009), it is not clear by looking only at the latest 5-year period if any trend is present.

While not appropriate to draw conclusions about trend when looking at the short timeframe of a 5-year period in this study, it can however be concluded that within this specific 5-year time period there is no trend evident. This is seen in figures 5.6 and 5.7 which show relatively similar peak percentages in 2018 and 2020, with similar although slightly higher SCA in 2021 and 2022. It can be seen that there are much higher snow cover levels in 2017 representing a better year for snow levels. While the data does provide interesting insight into SCA levels it is important to note that in this study SCA was only calculated four times a year representing each calendar season and that increased frequency of calculation could lead to more refined results and therefore more detailed conclusions of trend over the 5-year period. In addition to this it is also important to note that often calendar seasons do not align with peak and trough periods of snowfall and snow cover (Dye and Tucker, 2003) with snow often falling later in the winter season and melting mid to late Spring. This is confirmed by the SCA levels in figure 5.6 which show high SCA percentages for both Winter and Spring and Low values for Summer and Autumn. As a result, it is unlikely that results from this study provide an accurate insight into maximum SCA at greatest extent due to this period occurring sometime between winter and Spring.

Given these constraints which exist within the study some interesting insights can be gained from the aggregated images. The images show greatest extent for snow cover as well as reliability of covered area over the 5-year period. The results show only small portions of the study area are likely to be covered over all four seasons and with small amounts of variability between each year. It also shows, as in-line with expectation, that lower altitudes and larger extents covered in winter are often quite variable from season to season (Durand et al., 2009) with some specific regions of the study area only experiencing snow cover in winter for 2-3 seasons of the total 5.

Perhaps the most relevant observation which can be drawn from these images and one which would need to be confirmed with further analysis is that spring appears to be the most stable season with

relation to snow cover extent. By looking at comparisons between the other 3 seasons in figures 5.2, 5.3 and 5.5 and the spring season in figure 5.4 it can be seen that there are relatively few areas which are classified as being covered from 1-3 seasons when compared to a relatively large area which is covered by all 4 seasons. As a result, it might be suggested that this season may have the most stable SCA percentage. This is further backed up on analysis of the SCA percentage levels in table 5.1 with 3 out of the 4 years analysed falling within 1% point of one another and the 4th suffering from cloud cover masking. The reduced variability in SCA in this season, combined with a previous identification that shoulder seasons, being Spring, and Autumn, are most susceptible to the effects of climate change. This is due to factors such as early onset melt and delayed first snowfall (Dong, 2018) means that this season might be a prime candidate for more detailed and longitudinal studies to assess the effects of climate change on SCA levels in the European alpine region.

6.2 Accuracy assessment

The accuracy assessment gives an insight into the effectiveness and appropriateness of the classification methodology. While the study utilised two classification methodologies it is clear from the development of these only one is a reliable indication of the overall accuracy level of the classification, this being the error assessment utilising Planet data and performed in ENVI using a sample of the study area.

While the methodology utilised to calculate accuracy from the Météo-France data had advantages with relation to scalability and accuracy assessment of the entire data set, issues with relation to data quality and quantity posed problems with regard to carrying out such assessment. This has led to some seasons being classified with large over estimation of accuracy and some with large underestimations, while some would be considered accurate. This indicates that with further development of the methodology and utilisation of a much larger study area the methodology could provide more valid results which could be reliably used for accuracy assessment over a large timeframe. The relatively small study area compared with the Météo-France data coverage being the entire country (Météo-France, 2017) often led to only a small number of points being utilised in a classification leaving the assessment largely exposed to the effects of outliers in the data. In addition to this the unexpected factor of lack of data collection in many summer and autumn months led to difficulty producing accuracy assessment for these seasons. Again, it might be suggested that this methodology might be more appropriate for classifications which are occurring in Winter or Spring months when SCA levels are still high.

While these factors are important to note to ensure improvement in future studies, for the purposes of accuracy assessment in this study the results from the ENVI methodology will be relied upon. The

Research Report 43533710 Rhys Persoon

results of the accuracy assessments conducted over the four seasons were of an acceptable level and indicate that the classification yielded good results with all four classifications receiving overall accuracy levels above 90% (Gascoin et al., 2019).

6.3 Classification Methodology

Given the nature of the classification methodology and the relatively low levels of implementation of classification within Google Earth Engine previously, it is important to assess the results of the classification within the context of the generated accuracy assessment results, as well as discuss the limitations that have been imposed on the study. Overall, the classification was relatively successful with acceptable levels of error for all images generated, with accuracy levels achieved similar to other methodologies and an improvement upon automated classifications carried out by image providers (Gascoin et al., 2019). However, it is important to note the slightly higher levels of accuracy generated within images in months with reduced SCA levels. While more analysis would be required to confirm it is likely that this phenomenon is due to the high levels of complication when classifying snow cover in winter due to the effects of buildings, roads, and vegetation (Gascoin et al., 2019). While this project attempted to correct for some of these issues, including vegetation, it confirms that it is likely that the relatively simplistic method utilised to classify snow in the presence of higher levels of vegetation requires more development. This assessment has also been reached as snow cover classification that occurs in Summer and Autumn months often occurs at a higher elevation which is well above the tree line (Gascoin et al., 2019).

Other challenges that were experienced where related to the physical properties of the natural environment such as shading due to relief (Gaur et al., 2021). Which while not affecting classification to a large extent due to the methodology utilised, it is recognised that in a more in-depth study conducted, some more consideration should be given to the effects of such factors.

Finally, there were a number of challenges in the development of the method itself and the implementation within the GEE environment. This included limitations within the GEE environment relating to GEE coding specific practices, the nature of the way GEE undertakes image processing split between client and server-side operations complicating debugging, general limitation on capacity and data analysis within GEE, and limitations on the implementation of general coding conventions as well as remote sensing specific practices (Zhang and Zhang, 2020). In some cases, this may require a different methodology than originally proposed or a reduction in the scale of the analysis conducted to fit within the GEE processing framework and limitations (Zhang and Zhang, 2020).

7.0 Conclusions & Future Work

The project aimed to provide insight into snow cover area, in the specified region over the French alps, at a high-spatial resolution providing insight into the effects and changes of snow cover in this specific region from the mid-2010s onwards. In addition to this it was designed to provide an opportunity to not only assess the appropriateness and accuracy of existing classification methods but also build upon this foundation. This was done by implementing proven and tested methods and in some places combining these methods with others to improve overall results (Baral and Gupta, 1997). In this way the research built on the foundation of previous work to attempt to generate a more accurate and effective method of snow cover mapping in the European alpine region.

The results of this project combined with the implementation and further development of the use of GEE for SCA have also provided a basis in which further research in the area can be conducted. It has already been identified that there are a number of potential areas which require more study, and outcomes of this project suggest, that while challenges exist GEE for SCA is a viable and useful methodology that can be utilized to provide flexible, timely and accurate snow mapping. Key areas that can be researched in more depth in future work should include more detailed analysis with regards to temporal resolution by increasing the number of classified images within a year. Improving on the development of the already implemented classification methodology to better identify areas, including both vegetation cover and snow cover, to increase the accuracy of mapping in these areas. Improving the use of ground-based snow observations from weather monitoring stations for accurate and effective error analysis of all images within the study.

In addition to the above recommendations and refinements it is suggested that in future studies data outputs can be configured into the google application environment allowing for more dynamic location selection, time analysis, as well as improved visualization of the results. While this study has presented a number of ways to visualize the outputs of the analysis it is recognized that the time series data generated could also be displayed in a more interactive way to allow for improved understanding and analysis.

 The final recommendation for future work is to utilize methodologies developed in this study, as well as others, to conduct a longitudinal study potentially utilizing Landsat series imagery on snow cover loss in the Spring Season. This project has identified that there is potential to give more reliable results during this time period and the identified issues with snow cover loss during this particular time period in the European alpine region.

8.0 References

Baral, D. and Gupta, R., 1997. Integration of satellite sensor data with DEM for the study of snow cover distribution and depletion pattern. *International Journal of Remote Sensing*, 18(18), pp.3889-3894.

Boschetti, L., Stehman, S. and Roy, D., 2016. A stratified random sampling design in space and time for regional to global scale burned area product validation. *Remote Sensing of Environment*, 186, pp.465-478.

Callaghan, T., Johansson, M., Brown, R., Groisman, P., Labba, N., Radionov, V., Bradley, R., Blangy, S., Bulygina, O., Christensen, T., Colman, J., Essery, R., Forbes, B., Forchhammer, M., Golubev, V., Honrath, R., Juday, G., Meshcherskaya, A., Phoenix, G., Pomeroy, J., Rautio, A., Robinson, D., Schmidt, N., Serreze, M., Shevchenko, V., Shiklomanov, A., Shmakin, A., Sköld, P., Sturm, M., Woo, M. and Wood, E., 2011. Multiple Effects of Changes in Arctic Snow Cover. AMBIO, 40(S1), pp.32-45.

Congalton, R., 1991. A review of assessing the accuracy of classifications of remotely sensed data. *Remote Sensing of Environment*, 37(1), pp.35-46.

Dietz, A., Kuenzer, C., Gessner, U. and Dech, S., 2011. Remote sensing of snow – a review of available methods. *International Journal of Remote Sensing*, 33(13), pp.4094-4134.

Dong, C., 2018. Remote sensing, hydrological modelling and in situ observations in snow cover research: A review. *Journal of Hydrology*, 561, pp.573-583.

Dozier, J., 1989. Spectral signature of alpine snow cover from the landsat thematic mapper. *Remote Sensing of Environment*, 28, pp.9-22.

Durand, Y., Laternser, M., Giraud, G., Etchevers, P., Lesaffre, B. and Mérindol, L., 2009. Reanalysis of 44 Yr of Climate in the French Alps (1958–2002): Methodology, Model Validation, Climatology, and Trends for Air Temperature and Precipitation. *Journal of Applied Meteorology and Climatology*, 48(3), pp.429-449.

Dye, D. and Tucker, C., 2003. Seasonality and trends of snow-cover, vegetation index, and temperature in northern Eurasia. *Geophysical Research Letters*, 30(7).

European Space Agency, 2015. *Sentinel-2 User Handbook*. European Space Agency.

Farr, T., Rosen, P., Caro, E., Crippen, R., Duren, R., Hensley, S., Kobrick, M., Paller, M., Rodriguez, E., Roth, L., Seal, D., Shaffer, S., Shimada, J., Umland, J., Werner, M., Oskin, M., Burbank, D. and Alsdorf, D., 2007. The Shuttle Radar Topography Mission. *Reviews of Geophysics*, 45(2).

Gascoin, S., Grizonnet, M., Bouchet, M., Salgues, G. and Hagolle, O., 2019. Theia Snow collection: high-resolution operational snow cover maps from Sentinel-2 and Landsat-8 data. *Earth System Science Data*, 11(2), pp.493-514.

Gaur, M., Goyal, R., Saha, D., Singh, N., Shekhar, S., Ajai, A. and Chauhan, J., 2021. The Estimation of Snow Cover DistributionUsing Satellite Data in the Cold Arid Leh Regionof Indian Himalaya. *Polish Journal of Environmental Studies*, 31(1), pp.63-73.

Hall, D. and G. A, R., 2021. *MODIS/Terra Snow Cover 5-Min L2 Swath 500m, Version 61*. Boulder: NASA National Snow and Ice Data Center Distributed Active Archive Center.

Irshad, F., Malik, J. and Khalil, R., 2019. Mapping Wet Snow using SAR C-Band through Google Earth Engine. *2019 Sixth International Conference on Aerospace Science and Engineering (ICASE)*,.

Jain, S., Goswami, A. and Saraf, A., 2010. Snowmelt runoff modelling in a Himalayan basin with the aid of satellite data. *International Journal of Remote Sensing*, 31(24), pp.6603-6618.

Klein, G., Vitasse, Y., Rixen, C., Marty, C. and Rebetez, M., 2016. Shorter snow cover duration since 1970 in the Swiss Alps due to earlier snowmelt more than to later snow onset. *Climatic Change*, 139(3-4), pp.637-649.

Kokhanovsky, A., Lamare, M., Danne, O., Brockmann, C., Dumont, M., Picard, G., Arnaud, L., Favier, V., Jourdain, B., Le Meur, E., Di Mauro, B., Aoki, T., Niwano, M., Rozanov, V., Korkin, S., Kipfstuhl, S., Freitag, J., Hoerhold, M., Zuhr, A., Vladimirova, D., Faber, A., Steen-Larsen, H., Wahl, S., Andersen, J., Vandecrux, B., van As, D., Mankoff, K., Kern, M., Zege, E. and Box, J., 2019. Retrieval of Snow Properties from the Sentinel-3 Ocean and Land Colour Instrument. Remote Sensing, 11(19), p.2280.

Kumar, P., Husain, A., Singh, R. and Kumar, M., 2018. Impact of land cover change on land surface temperature: A case study of Spiti Valley. Journal of Mountain Science, 15(8), pp.1658-1670.

Li, B., Zhu, A., Zhou, C., Zhang, Y., Pei, T. and Qin, C., 2008. Automatic mapping of snow cover depletion curves using optical remote sensing data under conditions of frequent cloud cover and temporary snow. *Hydrological Processes*, 22(16), pp.2930-2942.

Li, J., Wang, L., Liu, S., Peng, B. and Ye, H., 2021. An automatic cloud detection model for Sentinel-2 imagery based on Google Earth Engine. *Remote Sensing Letters*, 13(2), pp.196-206.

Louis, J., Devignot, O. and Pessiot, L., 2021. *S2 MPC Level-2A Algorithm Theoretical Basis Document*. The European Space Agency.

Météo-France, 2017. Débuter avec le portail données publiques de Météo-France. Météo-France.

NASA, 2015. *The Shuttle Radar Topography Mission (SRTM) Collection User Guide*. NASA.

Olefs, M., Fischer, A. and Lang, J., 2010. Boundary Conditions for Artificial Snow Production in the Austrian Alps. *Journal of Applied Meteorology and Climatology*, 49(6), pp.1096-1113.

Pulliainen, J., Luojus, K., Derksen, C., Mudryk, L., Lemmetyinen, J., Salminen, M., Ikonen, J., Takala, M., Cohen, J., Smolander, T. and Norberg, J., 2020. Patterns and trends of Northern Hemisphere snow mass from 1980 to 2018. *Nature*, 581(7808), pp.294-298.

Rittger, K., Raleigh, M., Dozier, J., Hill, A., Lutz, J. and Painter, T., 2020. Canopy Adjustment and Improved Cloud Detection for Remotely Sensed Snow Cover Mapping. *Water Resources Research*, 56(6).

Salzano, R., Salvatori, R., Valt, M., Giuliani, G., Chatenoux, B. and Ioppi, L., 2019. Automated Classification of Terrestrial Images: The Contribution to the Remote Sensing of Snow Cover. *Geosciences*, 9(2), p.97.

Savoie, M., Armstrong, R., Brodzik, M. and Wang, J., 2009. Atmospheric corrections for improved satellite passive microwave snow cover retrievals over the Tibet Plateau. *Remote Sensing of Environment*, 113(12), pp.2661-2669.

Snapir, B., Momblanch, A., Jain, S., Waine, T. and Holman, I., 2019. A method for monthly mapping of wet and dry snow using Sentinel-1 and MODIS: Application to a Himalayan river basin. International Journal of Applied Earth Observation and Geoinformation, 74, pp.222-230.

Sokol, J., Pultz, T. and Walker, A., 2003. Passive and active airborne microwave remote sensing of snow cover. *International Journal of Remote Sensing*, 24(24), pp.5327-2344.

Tsai, Y., Dietz, A., Oppelt, N. and Kuenzer, C., 2019. Remote Sensing of Snow Cover Using Spaceborne SAR: A Review. *Remote Sensing*, 11(12), p.1456.

Vizzari, M., Santaga, F. and Benincasa, P., 2019. Sentinel 2-Based Nitrogen VRT Fertilization in Wheat: Comparison between Traditional and Simple Precision Practices. *Agronomy*, 9(6), p.278.

Zhang, D. and Zhang, L., 2020. Land Cover Change in the Central Region of the Lower Yangtze River Based on Landsat Imagery and the Google Earth Engine: A Case Study in Nanjing, China. *Sensors*, 20(7), p.2091.

Zhang, M., Huang, H., Li, Z., Hackman, K., Liu, C., Andriamiarisoa, R., Ny Aina Nomenjanahary Raherivelo, T., Li, Y. and Gong, P., 2020. Automatic High-Resolution Land Cover Production in Madagascar Using Sentinel-2 Time Series, Tile-Based Image Classification and Google Earth Engine. *Remote Sensing*, 12(21), p.3663.

Research Report   43533710   Rhys Persoon

9.0 Appendices

Appendix 1 – Google Earth Engine (GEE) Code

```
//  Properties
var TCol = {min:0, max:5000, bands:['B4','B3','B2']};    // Sets True Colour Image Display Properties
var ImgSet = 18                         // Selectes Image from sequence to display (between 0 and
18)
var dSeason = ee.Dictionary({                   // Stores which images related to which season
 '0.0': 'Sum_2017',
 '1.0': 'Aut_2017',
 '2.0': 'Win_2018',
 '3.0': 'Spr_2018',
 '4.0': 'Sum_2018',
 '5.0': 'Aut_2018',
 '6.0': 'Win_2019',
 '7.0': 'Spr_2019',
 '8.0': 'Sum_2019',
 '9.0': 'Aut_2019',
 '10.0': 'Win_2020',
 '11.0': 'Spr_2020',
 '12.0': 'Sum_2020',
 '13.0': 'Aut_2020',
 '14.0': 'Win_2021',
 '15.0': 'Spr_2021',
 '16.0': 'Sum_2021',
 '17.0': 'Aut_2021',
 '18.0': 'Win_2022'})


//  Sentinel 2 Collection Filtering

  // Loop to select indvidual seasons & filter based on geometry, cloud and band
var seasonFunction = ee.List.sequence(0, 54, 3).map(function(i) {
 var start = ee.Date('2017-06-01').advance(i, 'month')
 var end = start.advance(3, 'month')
 var Bandfilter = S2.select(['B1', 'B2', 'B3', 'B4', 'B5', 'B6', 'B7', 'B8', 'B8A', 'B9', 'B11', 'B12', 'AOT',
'WVP', 'SCL', 'TCI_R', 'TCI_G', 'TCI_B', 'QA10', 'QA20', 'QA60'])
 var Filtered = Bandfilter.filterDate(start,
end).filterBounds(geometry).filter(ee.Filter.lte('CLOUDY_PIXEL_PERCENTAGE', 30))

  // Generation of Cloud Mask and Cloudfree Image
  function maskS2clouds(image) {
  var qa = image.select('QA60')
  var cloudBitMask = 1 << 10;
  var cirrusBitMask = 1 << 11;
  var mask = qa.bitwiseAnd(cloudBitMask).eq(0).and(
        qa.bitwiseAnd(cirrusBitMask).eq(0))
  return image.updateMask(mask)
```

```
        .select(['B1', 'B2', 'B3', 'B4', 'B5', 'B6', 'B7', 'B8', 'B8A', 'B9', 'B11', 'B12', 'AOT', 'WVP', 'SCL', 'TCI_R',
'TCI_G', 'TCI_B', 'QA10', 'QA20', 'QA60'])
}
  var cloudMasked = Filtered.map(maskS2clouds)
  return ee.Image(cloudMasked.median().clip(geometry))
})
  // Assign to Image collection
var seasons = ee.ImageCollection.fromImages(seasonFunction)

// Calculating Indicies

var addIndex = function(img) {
  var ndsi = img.normalizedDifference(['B3','B11']).rename('ndsi');
  var ndvi = img.normalizedDifference(['B8','B4']).rename('ndvi');
  return img.addBands(ndsi).addBands(ndvi);
};
var with_Index = seasons.map(addIndex)

// Digital Elevation Model (DEM)

var elevation = DEM.select('elevation').clip(geometry)
  var elevationImg = ee.Image(0)                  // Generation of grouped elevation Image
    .where(elevation.gt(200), 200)
    .where(elevation.gt(400), 400)
    .where(elevation.gt(600), 600)
    .where(elevation.gt(800), 800)
    .where(elevation.gt(1000), 1000)
    .where(elevation.gt(1200), 1200)
    .where(elevation.gt(1400), 1400)
    .where(elevation.gt(1600), 1600)
    .where(elevation.gt(1800), 1800)
    .where(elevation.gt(2000), 2000)
    .where(elevation.gt(2200), 2200)
    .where(elevation.gt(2400), 2400)
    .where(elevation.gt(2600), 2600)
    .where(elevation.gt(2800), 2800)
    .where(elevation.gt(3000), 3000)
elevationImg = elevationImg.clip(geometry)

// Analysis

var indexN = ee.Number(0)
var IndexDisp =ee.ImageCollection(with_Index).toList(999)

var classifier = function(img) {

//     Snowline Estimate
  // Find SCA for each elevation group
```

Research Report   43533710   Rhys Persoon

```
  var snowBasline =
ee.Image(1).updateMask((ee.Image(ee.List(IndexDisp).get(indexN))).select('ndsi').gte(0.6))
  var Snowline = elevationImg.addBands(snowBasline).reduceRegion({
    reducer: ee.Reducer.count().group(0),
    geometry: geometry,
    scale: 100,
  })
  var SL_SVal = ee.List(Snowline.get('groups'))
    .map(function(i) {
     var dict = ee.Dictionary(i);
     return dict.get('count');
    });
 // Find total area for each elevation group
 var E_ZoneTot = elevationImg.addBands(elevationImg).reduceRegion({
    reducer: ee.Reducer.count().group(0),
    geometry: geometry,
    scale: 100,
  })
  var EL_SVal = ee.List(E_ZoneTot.get('groups'))
   .map(function(i) {
     var dict = ee.Dictionary(i);
     return dict.get('count');
   });
  // Perform snowline estimation calcuation
  var snowest = ee.List.sequence(0, 15).map(function(i) {
   var est_snowperc = (SL_SVal.getNumber(i).divide(EL_SVal.getNumber(i))).multiply(100)
   return est_snowperc
 })
 // Measure agaisnt cuttoff for snowline & and store for use in classification
 var lowperc = snowest.filter(ee.Filter.gt('item', 50)).get(0)
 var snowLineEle = ee.Number(snowest.indexOf(lowperc)).multiply(200)

 indexN = indexN.add(1)


//   Classification Decision

 // Classification cuttoffs for each of the stipulated criteria incluidng vegetation, water, elevation
and NDSI
 var individualclass = ee.Image(1)
   .where(img.select('ndvi').gte(0.8).and(img.select('ndsi').gte(0.4).and(img.select('B4').gte(3000))),
2)
   .where(DEM.gte(snowLineEle).and(img.select('ndsi').gte(0.4)).and(img.select('B4').gte(3000)),2)

.where(DEM.gte(snowLineEle).and(img.select('ndvi').gte(0.8).and(img.select('ndsi').gte(0.2).and(img.
select('B4').gte(3000)))),2)
   .where(img.select('ndsi').gte(0.6).and(img.select('B4').gte(3000)), 2)
   individualclass = individualclass.updateMask(img.select('B4').mask())
 return individualclass.clip(geometry)
```

```
}
var classified = with_Index.map(classifier)

//  Convert Image Collections to Image List to Return Single Images

var seasonsDisp=ee.ImageCollection(seasons).toList(999)

var IndexDisp =ee.ImageCollection(with_Index).toList(999)

var classDisp=ee.ImageCollection(classified).toList(999)


// Accuracy Assessment

var accuracyassessment = ee.List.sequence(0, 18).map(function(img) {
  var ISValData = ValDataIS.filterBounds(geometry)
var Dates = ee.Dictionary({
 '0.0': 'F2017_07',
 '1.0': 'F2017_10',
 '2.0': 'F2018_01',
 '3.0': 'F2018_04',
 '4.0': 'F2018_07',
 '5.0': 'F2018_10',
 '6.0': 'F2019_01',
 '7.0': 'F2019_04',
 '8.0': 'F2019_07',
 '9.0': 'F2019_10',
 '10.0': 'F2020_01',
 '11.0': 'F2020_04',
 '12.0': 'F2020_07',
 '13.0': 'F2020_10',
 '14.0': 'F2021_01',
 '15.0': 'F2021_04',
 '16.0': 'F2021_07',
 '17.0': 'F2021_10',
 '18.0': 'F2022_01'})

 // Compare CSV upload data against classified image where data is avaliable for the date
 var Date = Dates.get(img)
 var propImg = ISValData.filter(ee.Filter.rangeContains(Dates.get(img), 1, 2))
 var assessImg = ee.Image(ee.List(classDisp).get(img))
 var imgTest = assessImg.sampleRegions({
   collection: propImg,
   properties: [Dates.get(img)],
   tileScale: 16,
   scale: 20
 });
 var testConfusionMatrix = imgTest.errorMatrix(Dates.get(img), 'constant')
```

```
    return [testConfusionMatrix.accuracy()]
})
print(accuracyassessment)



//  Generation of Outputs

//      Calcualtion of SCA

  // Call individual images and group by snow area (SCA performed at scale 100m due to procressing
restrictions within GEE)
var SCAStat = ee.List.sequence(0, 18).map(function(img) {
  var snowArea =
ee.Image(ee.List(classDisp).get(img)).addBands(ee.Image(ee.List(classDisp).get(img))).reduceRegion(
{
    reducer: ee.Reducer.count().group(0),
    geometry: geometry,
    scale: 100,
  })
  var SnowAreaFormat = ee.List(snowArea.get('groups'))
    .map(function(i) {
      var dict = ee.Dictionary(i);
      return dict.get('count');
    });
  // Perform snow area classification
  var snowCoverArea = SnowAreaFormat.getNumber(1)
  var nonSnowArea = SnowAreaFormat.getNumber(0)
  var TotArea = snowCoverArea.add(nonSnowArea)
  var SCA = (snowCoverArea.divide(TotArea)).multiply(100)
  return SCA
})
print(SCAStat)

//    Generatio of SCA Chart

var chart = ui.Chart.array.values({
  array: SCAStat,
  axis:0,
  xLabels: dSeason.values()
}).setOptions({
  title: 'Snow Cover Area by Season',
  hAxis: {
    title: 'Season and Year',
    titleTextStyle: {italic: false, bold: true}
  },
  vAxis: {
    title: 'Snow Covered Area (% Total)',
    titleTextStyle: {italic: false, bold: true}
```

```
  },
  colors: ['1d6b99'],
  lineSize: 1,
  pointSize: 0,
  legend: {position: 'none'}
});
print(chart)

//   Aggregated Maps

var SummerImgs = ee.List.sequence(0, 18, 4).map(function(img) {
  return ee.Image(ee.List(classDisp).get(img))
})
var SummerAgg = ee.ImageCollection.fromImages(SummerImgs).sum()

var AutImgs = ee.List.sequence(1, 18, 4).map(function(img) {
  return ee.Image(ee.List(classDisp).get(img))
})
var AutAgg = ee.ImageCollection.fromImages(AutImgs).sum()

var WinterImgs = ee.List.sequence(2, 18, 4).map(function(img) {
  return ee.Image(ee.List(classDisp).get(img))
})
var WinterAgg = ee.ImageCollection.fromImages(WinterImgs).sum()

var SprImgs = ee.List.sequence(3, 18, 4).map(function(img) {
  return ee.Image(ee.List(classDisp).get(img))
})
var SprAgg = ee.ImageCollection.fromImages(SprImgs).sum()

var AllAgg = classified.sum()

// Mapping

Map.addLayer(ee.Image(ee.List(seasonsDisp).get(ImgSet)), TCol, 'True Colour');

Map.addLayer(ee.Image(ee.List(IndexDisp).get(ImgSet)), {min:0.4, max:1, bands:'ndsi',
palette:'Black, LightBlue'}, 'NDSI');
Map.addLayer(ee.Image(ee.List(IndexDisp).get(ImgSet)), {min:0, max:0.4, bands:'ndvi',
palette:'Black, Green'},'NDVI');

Map.addLayer(ee.Image(ee.List(classDisp).get(ImgSet)), {min:1, max:2},'Snow');

Map.addLayer(AllAgg, {min:18, max:50},'AllAggregate');
Map.addLayer(SummerAgg, {min:4, max:25},'SummerAggregate');
Map.addLayer(AutAgg, {min:4, max:25},'AutumnAggregate');
Map.addLayer(WinterAgg, {min:4, max:25},'WinterAggregate');
Map.addLayer(SprAgg, {min:4, max:25},'SpringAggregate');
```

Research Report   43533710   Rhys Persoon

```
//  Data Export - Change to Suit Data For Export

var Aggexport = SprAgg.toDouble()
var projection = Aggexport.projection().getInfo()
// ee.Image(ee.List(seasonsDisp).get(ImgSet)).projection().getInfo();
Export.image.toDrive({
  image: Aggexport,
  // ee.Image(ee.List(seasonsDisp).get(ImgSet)).select(['B4','B3','B2']),
  description: 'Indecies2',
  crs: projection.crs,
  region: geometry,
});
```